




The intrinsic chaperone network of Arabidopsis stem cells confers protection against proteotoxic stress

Ernesto Llamas¹ | Salvador Torres-Montilla² | Hyun Ju Lee¹ | María Victoria Barja² | Elena Schlimgen¹ | Nick Dunken³ | Prerana Wagle¹ | Wolfgang Werr⁴ | Alga Zuccaro³ | Manuel Rodríguez-Concepción^{2,5} | David Vilchez^{1,6,7} 

¹Cologne Excellence Cluster for Cellular Stress Responses in Aging-Associated Diseases (CECAD), University of Cologne, Cologne, Germany

²Centre for Research in Agricultural Genomics (CRAG) CSIC-IRTA-UAB-UB, Campus UAB Bellaterra, Barcelona, Spain

³Cluster of Excellence on Plant Sciences (CEPLAS), Institute for Plant Sciences, University of Cologne, Cologne, Germany

⁴Developmental Biology, Biocenter, University of Cologne, Cologne, Germany

⁵Institute for Plant Molecular and Cell Biology (IBMCP) CSIC-UPV, Valencia, Spain

⁶Center for Molecular Medicine Cologne (CMMC), University of Cologne, Cologne, Germany

⁷Faculty of Medicine, University Hospital Cologne, Cologne, Germany

Correspondence

David Vilchez, Cologne Excellence Cluster for Cellular Stress Responses in Aging-Associated Diseases (CECAD), University of Cologne, 50931 Cologne, Germany. Email: dvilchez@uni-koeln.de

Funding information

the European Research Council, Grant/Award Number: 677427; Deutsche Forschungsgemeinschaft, Grant/Award Number: 390661388

Abstract

The biological purpose of plant stem cells is to maintain themselves while providing new pools of differentiated cells that form organs and rejuvenate or replace damaged tissues. Protein homeostasis or proteostasis is required for cell function and viability. However, the link between proteostasis and plant stem cell identity remains unknown. In contrast to their differentiated counterparts, we find that root stem cells can prevent the accumulation of aggregated proteins even under proteotoxic stress conditions such as heat stress or proteasome inhibition. Notably, root stem cells exhibit enhanced expression of distinct chaperones that maintain proteome integrity. Particularly, intrinsic high levels of the T-complex protein-1 ring complex/chaperonin containing TCP1 (TRiC/CCT) complex determine stem cell maintenance and their remarkable ability to suppress protein aggregation. Overexpression of CCT8, a key activator of TRiC/CCT assembly, is sufficient to ameliorate protein aggregation in differentiated cells and confer resistance to proteotoxic stress in plants. Taken together, our results indicate that enhanced proteostasis mechanisms in stem cells could be an important requirement for plants to persist under extreme environmental conditions and reach extreme long ages. Thus, proteostasis of stem cells can provide insights to design and breed plants tolerant to environmental challenges caused by the climate change.

KEYWORDS

chaperones, heat stress, plant stem cells, protein aggregation, protein misfolding, proteostasis

1 | INTRODUCTION

Since proteins are involved in almost every biological process, protein homeostasis (proteostasis) is an essential requirement for cell physiology and viability. A complex network of cellular pathways

maintains the proper concentration, folding, and interactions of proteins from their synthesis through their degradation. As such, the proteostasis network assures the integrity and quality of the proteome, preventing cell malfunction and death. However, aging as well as metabolic, environmental, and pathological conditions can

This is an open access article under the terms of the Creative Commons Attribution License, which permits use, distribution and reproduction in any medium, provided the original work is properly cited.

© 2021 The Authors. *Aging Cell* published by Anatomical Society and John Wiley & Sons Ltd.



challenge the quality of the proteome in differentiated cells across tissues (Hipp et al., 2019; Powers et al., 2009; Vilchez et al., 2014; Wong & Cuervo, 2010).

Unlike most animals, plants exhibit a continuous supply of new and rejuvenated differentiated cells from the stem cell pools located in the root and shoot meristems (Weigel & Jurgens, 2002). For instance, the Sequoia tree contains stem cell reservoirs that can be active for more than 2,000 years (Scheres, 2007). As sessile organisms unable to remove themselves from persistent stressful environments (Heyman et al., 2014), this feature is particularly relevant to overcome ever-changing conditions. Plant stem cells give rise to new organs or rejuvenate and repair tissues, allowing the plant to persist amidst variable and extreme conditions (Dijkwel & Lai, 2019). Thus, defining molecular and cellular differences between stem cells and their differentiated counterparts could shed light on how plants can live many years even under variable environmental stress conditions (Dijkwel & Lai, 2019). In these lines, recent findings demonstrate that the shoot meristems of 200 years old oak trees are protected from the accumulation of deleterious mutations (Dijkwel & Lai, 2019; Schmid-Siebert et al., 2017). Given the essential role of proteostasis for cell function and viability, here, we asked whether plant stem cells have enhanced proteostasis mechanisms to maintain their biological function.

2 | RESULTS

2.1 | Root stem cells have increased ability to prevent accumulation of protein aggregates

To assess the proteostasis capacity of root stem cells of *Arabidopsis thaliana*, we used ProteoStat, a dye that becomes highly fluorescent when it binds to misfolded or aggregated proteins (Leeman et al., 2018; Nakajima & Suzuki, 2013; Shen et al., 2011). First, we performed a ProteoStat staining comparing seedlings grown under either control or distinct proteotoxic stress conditions that is proteasome inhibition (i.e., MG-132 treatment) and heat stress. In control seedlings, we did not detect aggregated proteins in most of the cells (Figure 1a and Figure S1). The only exception was the cell population forming the sloughing lateral root cap, a layer that is continuously replaced through programmed cell death (Shi et al., 2018) (Figure 1a and Figure S1). On the other hand, the seedlings subjected to proteotoxic stress exhibited high levels of aggregated proteins across differentiated cells of the root (Figure 1a) and cotyledons (Figure S2a–b).

Damaged proteins in roots under stress showed a particular distribution, as the stem cells next to the quiescent center (QC) had reduced amounts of protein aggregates compared with the rest of cells differentiating and expanding in opposite direction to the QC (Figure 1a–b). A closer magnification indicated that misfolded and aggregated proteins can be gradually detected as the differentiation of cortical cells advances in opposite direction to the QC (Figure 1c). Strikingly, cortical stem cells close to the QC showed undetectable protein aggregates (Figure 1c). To further examine the increased proteostasis ability of stem cells, we performed filter trap experiments

to monitor protein aggregation under heat stress. In particular, we focused on actin, one of the most abundant proteins in eukaryote cells which requires the assistance of chaperones for its proper folding (Vallin & Grantham, 2019). We found that differentiated cells exhibit a pronounced aggregation of actin under heat stress, whereas the stem cell region did not accumulate actin aggregates (Figure 1d). Together, our data suggest that plant stem cells have an enhanced ability to prevent protein misfolding and aggregation under stress conditions compared with their differentiated counterparts. Stress conditions not only induced protein aggregation in differentiated cells, but also impaired growth (Figure S3a–b). However, plants recovered growth after removal of the stress, suggesting that stem cells were able to restart their function to provide new pools of differentiated cells after maintaining their proteostasis under stress (Figure S4).

2.2 | CCT subunits are upregulated in the root tip containing stem cells

The chaperome network is a key node of proteostasis to prevent protein misfolding and aggregation (Brehme et al., 2014). In *Arabidopsis*, the chaperome network is formed by more than 300 chaperones and co-chaperones that regulate protein folding and aggregation under normal and stress conditions (Finka et al., 2011). To determine the molecular mechanisms that underlie the enhanced ability of stem cells to face proteotoxic stress, we analyzed available RNA-seq data from two different pools of root cells isolated by fluorescence-activated cell sorting (FACS) (Wendrich et al., 2017). By comparing root cells from the proximal part (mostly stem cells) and distal part (differentiated cells) respect to the QC (Figure 2a), we identified differentially expressed components of the chaperome network such as distinct chaperones, co-chaperones, and foldases in stem cells (Figure 2b). Undifferentiated stem cells displayed more and larger-magnitude transcriptional changes than their differentiated distal counterparts (Figure 2b, Data S1). Indeed, almost half (49.4%) of the chaperome network was significantly upregulated (\log_2 fold change >2 ; $p < 0.05$) in stem cells (Figure 2b, Data S1). On the other hand, 35.9% of the chaperome was significantly downregulated (\log_2 fold change <-2 ; $p < 0.05$) in these cells (Figure 2b, Data S1).

Remarkably, the transcriptomic analysis revealed that most members (88.9%) of the heat shock protein (HSP) 60 family, also known as chaperonins, were significantly increased in root stem cells (Figure 2b, Data S1). Among them, all the subunits of the T-complex protein-1 ring complex/chaperonin containing TCP1 (TRiC/CCT) complex were upregulated in root stem cells (Figure 2c, Data S1). Since the TRiC/CCT complex is also highly expressed in mammalian embryonic and adult stem cells (Noormohammadi et al., 2016; Vonk et al., 2020), we focused on this specific node of the chaperome network. First, we assessed the increased expression of CCT subunits by quantitative RT-PCR (qPCR) analysis of samples manually isolated from the root tip containing mainly stem cells in

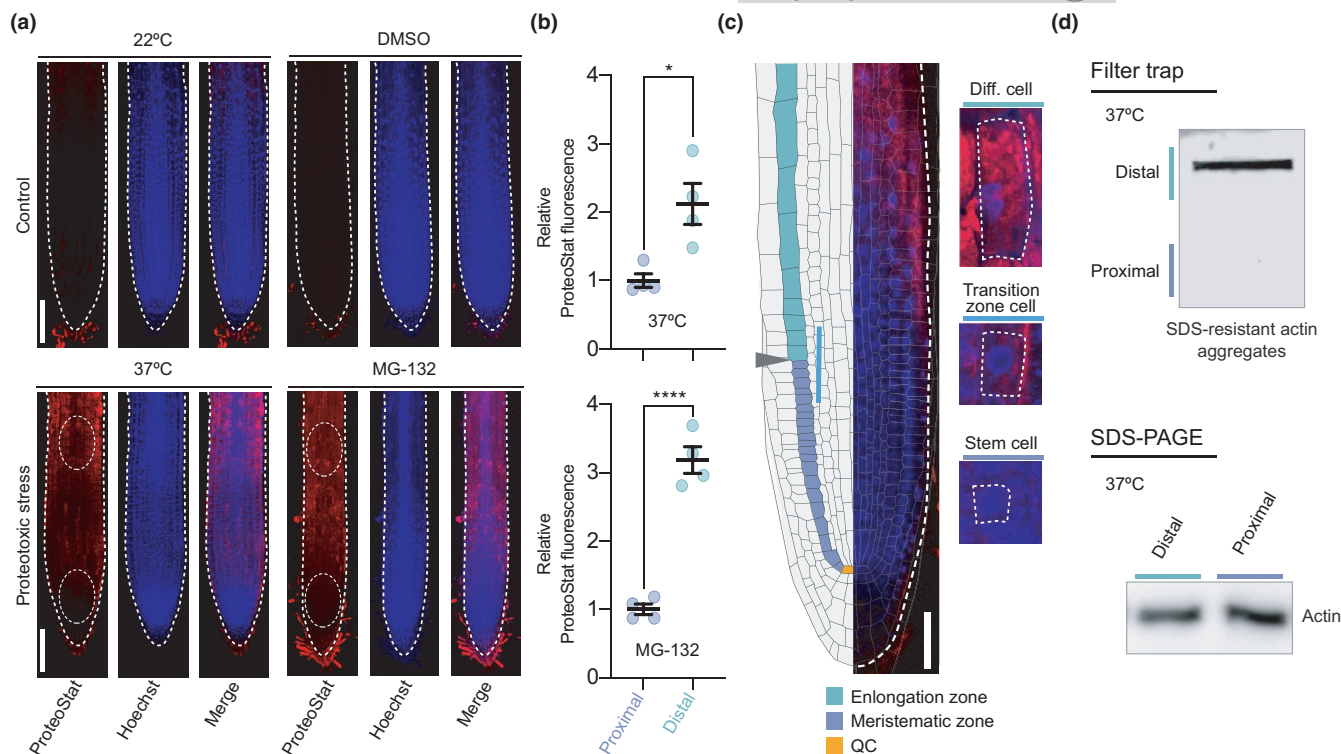


FIGURE 1 Proteotoxic stress causes differential protein aggregation in the distinct cell types of the root. (a) Representative images of wild-type plant roots grown under control (22°C or 22°C + DMSO) or proteotoxic stress conditions stained with ProteoStat Aggresome Detection kit. ProteoStat (red, protein aggregates), Hoechst (blue, nuclei), and Merge (ProteoStat and Hoechst) images are shown. For heat stress assay, 4 days after germination (DAG) plants were transferred to 37°C for 2 days. For proteasome inhibition experiments, plants were germinated and grown in plates supplemented with 30 μ M MG-132 and analyzed at 6 DAG stage. White bars represent 100 μ m. (b) Relative ProteoStat fluorescence levels comparing the area containing proximal (close to the QC) and distal cells from roots under proteotoxic stress (areas used for quantification are indicated with white dotted ovals in Figure 1a). Scatter plots represent mean \pm s.e.m. of four independent experiments. The statistical comparisons were made by two-tailed Student's *t* test for unpaired samples. *p* values: **p* < 0.05, *****p* < 0.0001. (c) Left side, scheme indicating the structure of the Arabidopsis root meristem. The QC is indicated in orange color, the meristematic zone in green, and the elongation zone in purple. Gray arrowhead indicates the transition zone, where cells leave the meristem and enter the elongation/differentiation zone. Right side, close examination of a representative MG-132-treated root showing differential protein aggregation in cortical cells dividing and differentiating in opposite direction to the QC. White bar indicates 50 μ m. (d) Filter trap and SDS-PAGE analysis with antibody to actin of the areas containing proximal and distal cells from roots under proteotoxic stress (37°C for 2 days). The images are representative of two independent experiments

comparison with the root base and the shoot, both of them containing mainly differentiated cells (Figure 2d). The qPCR analysis of root meristem maintenance marker genes (i.e., *PLT2* (AT1G51190) and *TMO7* (AT1G74500)) confirmed that the distinct collected tissues contained different proportions of stem and differentiated cells (Figure 2e). Both marker genes showed a gradient of expression with a maximum in the root stem cells (Durgaprasad et al., 2019; Wendrich et al., 2017), as we observed in root tip samples (Figure 2e). Likewise, qPCR analysis indicated that *CCT* transcripts are expressed at higher levels in the root tip compared with differentiated tissues (Figure 2f). To further support increased expression of *CCT* subunits in stem cells, we calculated the ratio between individual *CCT* and *TMO7* transcripts levels obtained from each isolated root tissues, and we found that *CCT/TMO7* ratios were consistently higher in root tips compared with the root base (Figure 2g). Importantly, Western blot analysis confirmed that the higher mRNA

levels of *CCT7* correlated with higher amounts of the protein in the root tip (Figure 2h). In addition, the Plant eFP Viewer (bar.utoronto.ca), a bioinformatic tool that displays gene expression patterns, indicates higher expression levels of all the *CCT* genes in the root stem cell niche (Figure S5a). This analysis also shows enhanced expression of *CCT* genes in the meristematic zone enriched for stem cells of the xylem when compared with vascular cells of the distal xylem that have undergone a gradual differentiation process along the root (Figure S5b). Altogether, our data indicate that root plant stem cells have an intrinsic chaperome network characterized by enhanced levels of *CCT* subunits, a feature that could contribute to their enhanced ability to prevent protein aggregation under proteotoxic stress. Importantly, *CCT* transcripts were not upregulated in the root after heat stress treatment (Figure S6), suggesting that the basal high expression of *CCTs* is sufficient to prevent proteostasis collapse under stress conditions.

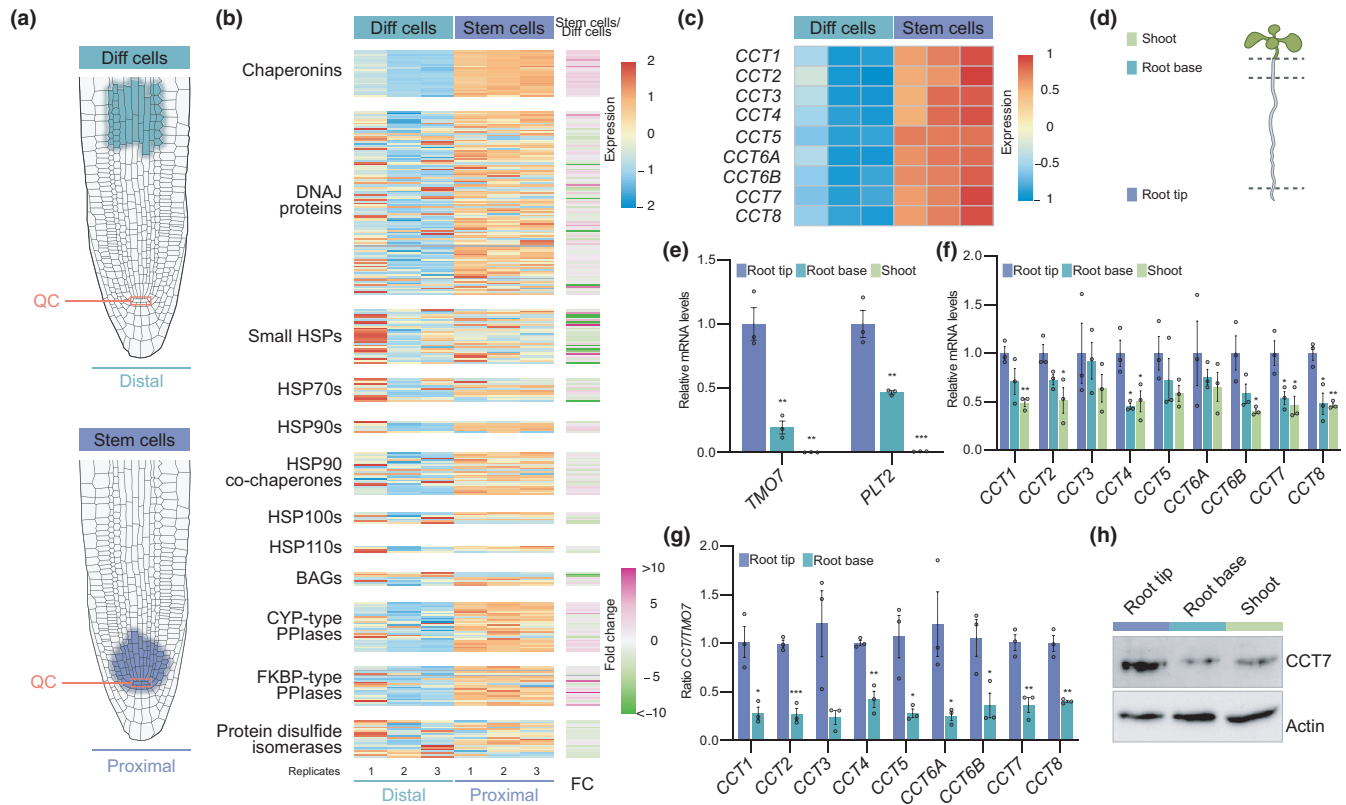


FIGURE 2 Chaperonin containing TCP1 subunits are upregulated in the root tip containing stem cells. (a) Diagram depicting cell populations in the proximal zone (stem cells) and distal zone (differentiated cells) respect to the QC of the root apical meristem. Data for RNA-seq analysis were obtained from the indicated proximal and distal cells isolated by FACs (Wendrich et al., 2017). (b) Heatmap representing expression (fragments per kilobase of transcript per million, FPKM) and fold change expression of chaperome component transcripts comparing stem cells (proximal zone) with differentiated cells (distal zone) (log₂ fold change (FC) > 2, $p < 0.05$ was considered significant). The chaperome genes were divided into different groups: Chaperonins (HSP60s), DNAJ proteins, small HSPs, HSP70s, HSP90s, HSP90 co-chaperones, HSP100s, HSP110s, BAGs, CYP-type peptidyl-proline isomerases (PPIases), FKBP-type PPIases, and protein disulfide isomerase as defined by Finka et al., 2011. (c) Heatmap showing expression levels (FPKM) of all CCT subunits. Both FPKM heatmaps are row-scaled. (d) Scheme depicting the different sections of wild-type plants at 6 DAG. Isolated shoot (green), root base (blue), and root tip (purple) were used for RNA and protein extraction. (e) qPCR analysis of transcript levels of genes that are highly expressed in stem cells to regulate root meristem maintenance (mean \pm s.e.m of 3 independent experiment). (f) qPCR analysis of transcript levels of the indicated CCT subunits relative to levels in the root tip (mean \pm s.e.m of 3 independent experiment). (g) CCT/TMO7 ratio in root tip and root bases samples (mean \pm s.e.m of 3 independent experiment). (h) Western blot analysis with antibody against CCT7 subunit. Actin is the loading control. The images are representative of three independent experiments. All the statistical comparisons in (e, f and g) between samples from root tip and differentiated cells were made by two-tailed Student's *t* test for unpaired samples. p value: * $p < 0.05$, ** $p < 0.01$, *** $p < 0.001$

2.3 | Reduced levels of CCT trigger protein aggregation in root stem cells and impairs stem cell function

Intrigued by the intrinsic high levels of CCT subunits in root stem cells, we asked whether TRIC/CCT determines stem cell function and viability. Since loss of a single CCT subunit is sufficient to impair the assembly and activity of the TRIC/CCT complex (Ahn et al., 2019; Gonczy et al., 2000; Green et al., 2011; Lundin et al., 2008), we assessed whether an unbalance in the expression of CCT subunits impairs stem cell activity and subsequent root growth. To this end, we performed a root growth screening among Arabidopsis T-DNA mutants from genes encoding CCT subunits. We first isolated and characterized two insertion alleles for CCT4, CCT7, and CCT8 subunits (Figure S7a). T-DNA insertions in the promoter of CCT4 (*cct4-1* and

cct4-2) or CCT7 (*cct7-1*) led to slightly reduced expression, whereas insertions in transcribed but untranslated regions of CCT7 (*cct7-2*) and CCT8 (*cct8-2* and *cct8-4*) caused a stronger reduction in transcript levels (Figure S7b–c). Thus, we classified the mutants as weak (*cct4-1*, *cct4-2*, and *cct7-1*) and moderate loss of function (*cct7-2*, *cct8-2*, and *cct8-4*). While we did not observe root growth effects in weak mutants, all the moderate mutant lines exhibited shorter roots compared with wild-type (WT) controls (Figure S8). In addition, we also examined the root length of mutants with alterations in the prefoldin (PFD) complex (Grantham, 2020), a distinct molecular chaperonin which is also highly expressed in stem cells (Figure 2b, Data S1). Importantly, PFD and TRIC/CCT complex interact and act together to facilitate folding of numerous proteins (Martin-Benito et al., 2002). Similar to moderate *cct7-2*, *cct8-2* and *cct8-4* mutants, *pdf3* and *pdf5* mutants showed shorter roots compared with the WT

seedlings (Figure S8). Thus, our data indicate that TRiC/CCT along with PFD complex contribute to proper maintenance of the meristem and subsequent continuous root growth.

Given that null mutations of CCT subunits are lethal in plants, yeast, and mammals (Horwich et al., 2007; Xu et al., 2011), the moderate loss-of-function mutants *cct7-2* and *cct8-2* provide an invaluable mean to study proteostasis and stem cell maintenance. We further characterized these *cct* mutants and found that the root growth was impaired over time (Figure 3a). Moreover, mutations in CCT genes led to a reduced number of cortical cells in the meristem, resulting in shorter meristems (Figure 3b–c). Notably, *cct7-2* and *cct8-2* mutant plants displayed a disordered stem cell niche with aberrant cellular organization and division planes in the columella root cap and the QC (Figure 3c). Prompted by these results, we tested whether downregulation of CCT levels alter expression of markers

of stem cell maintenance. To this end, we compared the transcript levels of *PLT2* and *TMO7* between WT, *cct7-2*, and *cct8-2* plants. Notably, we found lower levels of *PLT2* and *TMO7* in the *cct* mutant seedlings (Figure S9).

We hypothesized that the imbalance in the TRiC/CCT complex of *cct* mutants could lead to aberrant protein aggregation in stem cells, a process that impairs cell function. To assess this possibility, we used ProteoStat staining. Notably, we found increased protein aggregation in the stem cell niche of *cct* mutant plants compared with WT controls (Figure 3d–e). Moreover, a closer examination of the cortical stem cell region allowed us to detect fluorescence speckles in stem cells, indicating protein aggregation (Figure 3f). Since actin is a major folding substrate of the TRiC/CCT complex (Vallin & Grantham, 2019), we assessed actin aggregation in *cct8-2* plants. Notably, we found that loss of *cct8* function triggers actin aggregation (Figure 3g).

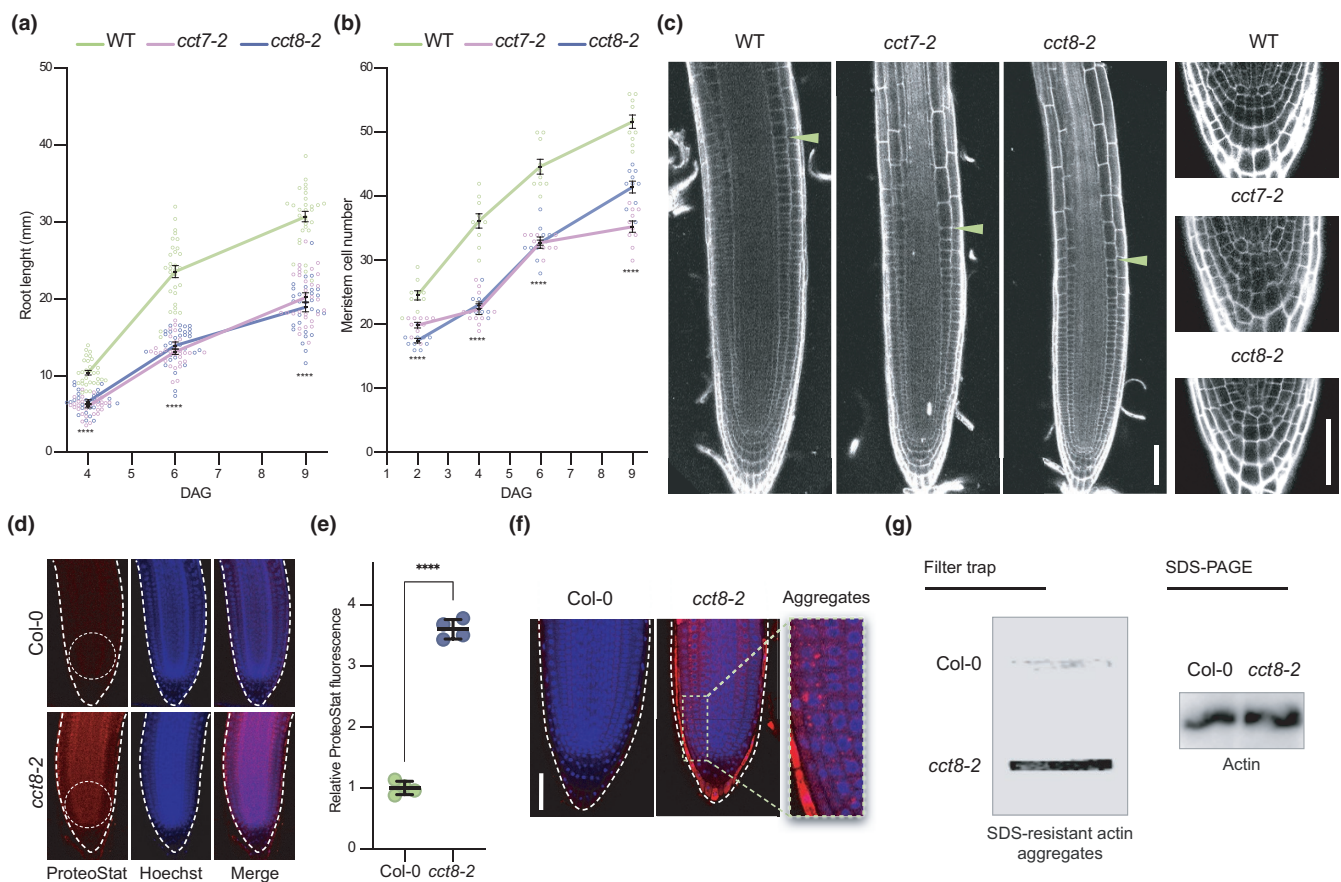


FIGURE 3 Reduced expression of CCT triggers protein aggregation in root stem cells and impairs stem cell function. (a) Root length over time in wild-type (WT), *cct7-2*, and *cct8-2*. DAG, days after germination ($n = 30$ roots from three independent experiments). (b) Meristem cell number over time in WT, *cct7-2*, and *cct8-2* ($n = 10$ roots from three independent experiments). In (a–b) staggered plot showing connecting lines to the means. (c) Representative images of propidium iodide (PI)-stained roots show differences between the meristem size of Col-0 WT and *cct* roots at 4 DAG. Green arrowheads indicate the junction between the meristematic and elongation zone. Lower panels show a magnification to the QC and columella cells. Scale bars represent 50 μm . (d) Representative images of ProteoStat staining of Col-0 WT and *cct8-2* mutant at 6 DAG. Seedlings were grown under control conditions (22°C). Scale bar represents 50 μm . (e) Relative ProteoStat fluorescence levels within the area containing proximal cells (close to the QC) of *cct8-2* relative to Col-0 control (mean \pm s.e.m. of 4 independent experiments). The areas used for quantification are indicated with white dotted ovals in Figure 3d. (f) Higher magnification of the stem cell niches of Col-0 and *cct8-2*. Scale bar represents 50 μm . (g) Filter trap and SDS-PAGE analysis with antibody to actin of Col-0 and *cct8-2* plants. The images are representative of two independent experiments. All the statistical comparisons in (a, b and e) were made by two-tailed Student's *t* test for unpaired samples. p value: **** $p < 0.0001$



Altogether, these data establish a link between proteostasis, TRiC/CCT complex activity, and root stem cell maintenance.

2.4 | Overexpression of CCT8 confers resistance to proteotoxic stress in plants

During organismal aging, differentiated cells of animals undergo a progressive decline in their proteostasis network, losing their ability to

maintain proteome integrity and cope with proteotoxic stress (Lopez-Otin et al., 2013; Taylor & Dillin, 2011). However, mammalian embryonic stem cells rely on enhanced proteostasis mechanisms to replicate indefinitely while maintaining their undifferentiated state and, therefore, are immortal in culture (Noormohammadi et al., 2016; Vilchez et al., 2012; Vilchez et al., 2012). Since our results indicate that plant stem cells also exhibit enhanced proteostasis, we asked whether mimicking root stem cell proteostasis in somatic tissues confers organismal protection to proteotoxic stress. For this purpose, we

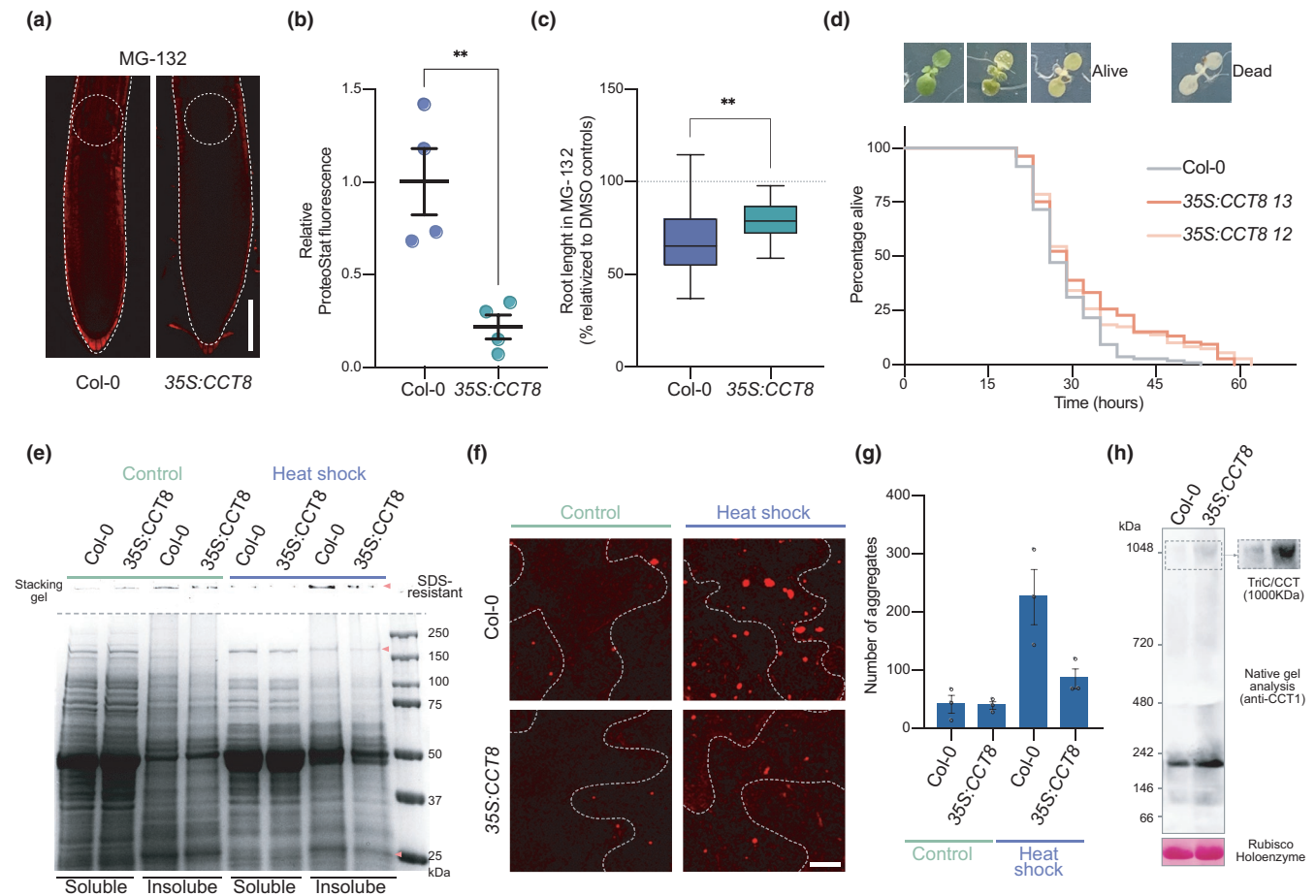


FIGURE 4 Overexpression of CCT8 is sufficient to ameliorate protein aggregation in differentiated cells and confer resistance to proteotoxic stress in plants (a) Representative images of ProteoStat staining of 6 DAG Col-0 and 35S:CCT8 germinated and grown in plates supplemented with 15 μM MG-132. Scale bar represents 100 μm. (b) Relative ProteoStat fluorescence levels comparing the areas depicted with white dotted circles in Figure 4a. Graph represents mean ± s.e.m of four independent experiments. (c) Root lengths of MG-132-treated plants relative to their corresponding controls treated with DMSO. Statistical comparisons in (b–c) were made by two-tailed Student's *t* test for unpaired samples. *p* value: ***p* < 0.01. (d) Heat shock survival assay of 35S:CCT8 plants and Col-0 WT. 6 DAG seedlings grown at 22°C were subject to 45°C for 3 h (heat shock) and then shifted back to control conditions (22°C). Alive plants were scored. Dead plants were counted when they showed a complete pigment bleaching phenotype. Kaplan–Meier survival data are representative of 2 independent experiments. All lines were grown in the same plate. 35S:CCT8 12 (log rank, *p* < 0.00138) and 35S:CCT8 13 (log rank, *p* < 0.00151) survive longer than control seedlings under heat stress. Col-0 WT: median = 26, *n* = 76/108, 35S:CCT8 12: median = 29, *n* = 59/108. 35S:CCT8 13: median = 29. (e) Representative BlueSafe-stained SDS-PAGE gel of protein extracts from the soluble and insoluble fractions. Insoluble/aggregated protein bands that show strong decreased in heat stress-treated 35S:CCT8 plants compared with heat stress-treated WT are indicated with orange arrowheads. SDS-resistant aggregates retained on the stacking gel are also shown. (f) Plants from the heat shock assay were stained with ProteoStat and representative images are shown. Scale bar represents 10 μm. (g) Quantification of the number of aggregates stained with ProteoStat. Total number of aggregates were counted in the whole 63X captured image from the epidermis of the cotyledons (mean ± s.e.m from 3 independent experiments). (h) Representative images of two independent native gel electrophoresis of Col-0 WT and 35S:CCT8 extracts collected from 14 DAG plants followed by immunoblotting with CCT1 antibody (right panel shows the TRiC/CCT complex band with longer exposure time). Band corresponding to Rubisco holoenzyme after Ponceau staining is the loading control



overexpressed CCT8, a subunit that is sufficient to increase TRiC/CCT assembly in both human cells and the roundworm *Caenorhabditis elegans* (Noormohammadi et al., 2016). We generated two independent transgenic lines that express upregulated levels of CCT8 (Figure S10) and assessed resistance to proteotoxic stress. Notably, we found that CCT8-overexpressing plants accumulate less aggregates in roots compared with wild-type plants when both were treated with MG-132 proteasome inhibitor (Figure 4a–b), resulting in longer roots under this deleterious condition (Figure 4c). In addition, stress-challenged transgenic lines displayed extra cell layers in the sloughing lateral root cap that is normally subject to continuous cell death and replacement (Figure S11a). This phenotype could be caused by the constitutive CCT8 expression during the columella differentiation process, in which the levels of endogenous CCT8 transcript decay (Figure S11b–c). Besides proteasome inhibition, we also assessed the effects on heat stress in the shoot of CCT8-overexpressing plants. To this end, we performed a heat shock survival assay where 6 day after germination (DAG) seedlings were subjected to 3 h of 45°C heat shock and then shifted back to 22°C. We found that 35S:CCT8 plants exhibit increased survival after heat shock compared with wild-type plants (Figure 4d). Since heat shock triggers the accumulation of misfolded and aggregated proteins that can cause cell death, enhanced survival after heat shock may be explained by reduced protein aggregation in 35S:CCT8 plants. In support of this hypothesis, soluble and insoluble protein analysis as well as ProteoStat staining confirmed that 35S:CCT8 seedlings contained less protein aggregates after heat shock (Figure 4e–g). By native gel analysis, we confirmed that TRiC/CCT complex assembly was enhanced in plants upon CCT8 overexpression (Figure 4h). Thus, our data indicate that upregulation of CCT8 and subsequent assembly of TRiC/CCT complex confers protection to heat stress by sustaining the integrity of the proteome.

3 | DISCUSSION

The cells of all living organisms contain numerous proteins which are at risk of misfolding and aggregation (Balchin et al., 2016; Knowles et al., 2014). The accumulation of damaged proteins can lead to defects in growth, decrease in yield, accelerated aging, and cellular death (Planas-Marques et al., 2016). A series of tightly regulated and stringent mechanisms maintain proteostasis (Hipp et al., 2019; Vilchez et al., 2014). However, aging, metabolic conditions, and environmental challenges can overwhelm the proteostasis network. For example, protein aggregation in aging neurons is linked with several human neurodegenerative disorders such as Alzheimer's, Parkinson's, and Huntington's disease (Douglas & Dillin, 2010; Lee et al., 2017; Lopez-Otin et al., 2013). Likewise, stress conditions can induce proteostasis collapse and protein aggregation in plants (Llamas et al., 2017; Nakajima & Suzuki, 2013; Pulido et al., 2016). We found that maintaining low levels of protein aggregation during stress conditions contribute to plant stem cell viability, ensuring tissue rejuvenation by cellular replacement as well as continuous and repetitive formation of new structures and organs. In these lines,

our results indicate that root stem cells have an enhanced protein folding capacity, providing them with a striking ability to cope with proteotoxic stress compared with their differentiated counterparts. For instance, similar to animal stem cells (Noormohammadi et al., 2016; Thiruvalluvan et al., 2020; Vonk et al., 2020), we identified distinct components of the Arabidopsis chaperome upregulated in stem cells, such as DNAJs, HSPs, and peptidyl-proline isomerases (PPIases). Particularly, we found a strong enrichment in the levels of distinct members of the chaperonin family in plant stem cells, including all the CCT subunits of the TRiC/CCT complex.

Plant and animal stem cells have unexpected similarities that modulate their function (Sablowski, 2004). One classic paradigm is the conserved protein retinoblastoma (Rb), which is critical for cell division and differentiation of plant and animal stem cells (Sablowski, 2004; Scheres, 2007). In addition, genome stability maintains a healthy pool of stem cells in both plants and animals (Schmid-Siebert et al., 2017; Zheng, 2020). Recently, it has been reported that stem cells of the shoot meristem are robustly protected from the accumulation of mutations in long-lived trees (Schmid-Siebert et al., 2017). Besides cell division and genome stability, our results establish that both plant and animal stem cells rely on a powerful proteostasis machinery for their function and maintenance (Lee et al., 2017).

Whereas a collapse in the proteostasis of terminally differentiated cells can lead to disease, human, and mouse stem cells exhibit an enhanced ability to correct proteostatic deficiencies. For instance, pluripotent and adult stem cells have increased proteolytic systems and expression of distinct chaperones to prevent protein misfolding and aggregation (Leeman et al., 2018; Llamas et al., 2020; Noormohammadi et al., 2016, 2018; Prinsloo et al., 2009; Thiruvalluvan et al., 2020; Vilchez et al., 2012, 2013; Vonk et al., 2020). Interestingly, mimicking proteostasis of human pluripotent stem cells by ectopically increasing CCT8 in somatic tissues can suppress the aggregation of disease-related proteins such as polyQ-expanded huntingtin, the mutant protein underlying Huntington's disease (Noormohammadi et al., 2016). Besides CCT subunits, we found that plant stem cells have increased levels of distinct PPIases including cyclophilins (CYPs) and FK506-binding proteins (FKBPs) (Figure 2b). Importantly, CYPs and FKBPs facilitate the proper folding and prevent aggregation of human pathogenic proteins such as the prion protein (PrP) and presenilin 1, which is linked with familial Alzheimer's disease (Cohen & Taraboulos, 2003; van de Hoef et al., 2013; Wang et al., 2005). Thus, the endogenous upregulation of chaperonins and other proteostasis components such as PPIases could be a conserved mechanism to increase protein folding activity and maintain proteome integrity, ensuring the survival of stem cells. Moreover, due to the larger number of chaperone members in plants compared to humans (Finka et al., 2011), we speculate that plant chaperones could be used as therapeutic targets against human pathogenic proteins to ameliorate neurodegenerative diseases.

Animals exhibit a series of intracellular and cell-nonautonomous mechanisms that allow them to respond differently to acute stress (e.g., heat shock) or chronic stress ensued by aging or the expression of misfolded mutant proteins (Taylor et al., 2014). In animals



such as *C. elegans*, the ability to induce the heat shock response in specific tissues comes at the expense of the organismal ability to maintain proteostasis in the face of chronic proteotoxic stress (Prahlad & Morimoto, 2011; Volovik et al., 2014). In contrast to animals, plants cannot escape from temperature fluctuations in nature and have evolved different strategies to cope with recurring environmental stress. For instance, plants can be primed with moderate heat stress, which triggers the activation of heat shock transcription factors (HSFs) and subsequent upregulated expression of heat shock proteins (HSPs). This prime response can last several days enabling plants to survive temperatures that otherwise would be lethal for an unadapted plant (Baurle, 2016). However, when plants are exposed to unexpected long or chronic stress episodes, they must have additional mechanisms to maximize survival. As sessile organisms, maintenance of plants stem cell reservoirs is critical to continuously supply new and rejuvenated differentiated cells in damaged organs or directly generate new organs to replace them (Weigel & Jurgens, 2002). Thus, preventing protein misfolding and aggregation in plant stem cells before, during and after stress conditions can be an important requirement for stem cell viability and function. As such, the enhanced proteostasis network of stem cells could allow the plant to keep growing during stress or regenerate after removal of the stress. This could be a potential explanation to why CCT genes, as many other chaperonins, are constitutively highly expressed in plant stem cells (Figure 2) and why their expression is independent of the heat stress response (Figure S6). In these lines, we speculate that the enhanced proteostasis of plant stem cells contribute to the extreme ages that distinct plants are able to achieve, even when they are continuously exposed to abiotic stresses such as high temperature (Weigel & Jurgens, 2002). While very few mammals, including humans, can live more than 100 years, plants like the bristlecone pine and the giant sequoia are able to live over a 1,000 years (Dijkwel & Lai, 2019; Heyman et al., 2014; Scheres, 2007), probably due to their stem cell pools (Heyman et al., 2014). Remarkably, we found that mimicking the proteostasis network of stem cells in somatic tissues by increasing TRiC/CCT assembly is sufficient to prevent protein aggregation in differentiated cells and increase organismal survival under stress conditions. However, further studies will be required to assess whether this upregulated ability to cope with acute heat stress could eventually jeopardize proteostasis under chronic stress as it occurs in animals. Nevertheless, our results indicate that rewiring proteostasis mechanisms in crop plants could have an important agronomic value to maintain yield in the face of unpredictable daily temperature fluctuations due to the global climate change.

Given that CCT subunits are expressed constitutively under normal growth conditions in eukaryotes (Simmer et al., 2003), an intriguing question raised by our results is how plant stem cells maintain elevated levels of CCT subunits compared with differentiated cells. Similar to our findings, previous studies in yeast have demonstrated that, unlike most chaperones, the expression of CCT genes is not induced by heat shock and associated transcription factors such as HSFs (Somer et al., 2002; Ursic & Culbertson, 1992).

Interestingly, the TF2Network that predicts potential regulators of sets of co-expressed or functionally related genes in plants (Kulkarni et al., 2018), indicates that most of the CCT genes could be modulated by the zinc finger transcription factor GATA12 (AT5G25830) (Figure S12a). Similar to CCT genes, the expression of GATA12 is also upregulated in stem cells when compared to differentiated cells (Figure S12b–c). Thus, it will be fascinating to examine in further studies whether GATA12 transcription factor modulates the high expression levels of CCT subunits. In these lines, it is important to note that human embryonic stem cells also express higher amounts of CCT subunits compared with their differentiated counterparts (Noormohammadi et al., 2016). Likewise, adult stem cells such as mouse neural stem cells and *C. elegans* germline stem cells also have enhanced expression of CCT subunits (Noormohammadi et al., 2016; Vonk et al., 2020). The regulatory mechanisms underlying elevated CCT levels in these models remain unknown, but we speculate that specific transcription factors could cross evolutionary boundaries to promote high levels of CCT subunits and subsequent assembly of the TRiC/CCT complex in distinct stem cells of different species.

4 | EXPERIMENTAL PROCEDURES

4.1 | Plant material, constructs, and growth conditions

All the *Arabidopsis thaliana* lines used in this work are in Columbia-0 (Col-0) ecotype. Wild-type, and loss-of-function mutants *cct4-1* (SALKSEQ_069998.1), *cct4-2* (SALKSEQ_076214.0), *cct7-1* (SALKSEQ_135744.2), *cct7-2* (SALK_099986), *cct8-2* (SALKSEQ_082168)(Xu et al., 2011), *cct8-4* (SALKSEQ_137802), *pdf3* (Rodriguez-Milla & Salinas, 2009), and *pdf5* (Rodriguez-Milla & Salinas, 2009) were used in this study. T-DNA mutants were genotyped by PCR. All seeds were surface-sterilized and germinated on solid 0.5X Murashige and Skoog (MS) medium without sucrose neither vitamins, and plants were incubated in a growth chamber at 22°C (or otherwise indicated in the figure) under long-day conditions as previously described (Pulido et al., 2013). When indicated in the figure, medium was supplemented with MG-132 (Sigma). For the root growth analysis, we used the software MyRoot to semi-automatically measure the root length from 6 day after germination (DAG) seedlings grew in vertical agar plates (Betegon-Putze et al., 2019). For qPCR, filter traps and Western blot analysis of the root tip, base root and shoot, seeds were germinated on vertical plates with a sterile mesh (SefarNitex 03-100/44) placed on the medium. 6 DAG plants were dissected manually with a surgical blade for posterior RNA and protein extraction. For the generation of the 35S:CCT8 lines, the full-length coding sequence of Arabidopsis CCT8 (AT3G03960) was cloned under the 35S promoter using the entry vector pDONR207 and the destination vector pGWB502. Arabidopsis plants were transformed by the floral dip method (Clough & Bent, 1998).



4.2 | Analysis of RNA-seq data

We analyzed publicly available RNA-Seq data from two different pool of cells isolated by FACS from Arabidopsis roots of the lines *PUB25* and *SPT*. We used the RNA-sequencing samples *PUB25* proximal 1–3 (corresponding to mainly stem cells) and *SPT* distal 1–3 (corresponding to differentiated vascular cells) (Wendrich et al., 2017) to compare the expression profile of the Arabidopsis chaperome as defined by Finka et al., 2011. RNA-seq data were analyzed using a QuickNGS pipeline (Wagle et al., 2015). This workflow system provided a basic read quality check using FastQC (version 0.10.1) and read statistics using SAMtools (version 0.1.19). The basic data processing of the QuickNGS pipeline consists of a splicing-aware alignment using Tophat2 (version 2.0.10) followed by reference-guided transcriptome reassembly with Cufflinks2 (version 2.1.1). The QuickNGS pipeline calculated read count means, fold change, and *p* values with DESeq2 and gene expression for the individual samples with Cufflinks2 (version 2.1.1) as fragments per kilobase of transcript per million (FPKMs), in both cases using genomic annotation from the Ensembl database, version 32. All data preprocessing and visualization were done with R version 3.2.2 and Bioconductor version 3.0. Differential expressed genes (DEGs) calculated by DESeq2 were filtered using *p* value <0.05 cutoff of significance, and log₂ fold change >2 and log₂ fold change <-2 cutoffs of relative expression for upregulated and downregulated DEGs, respectively. Heatmaps were created using "pheatmap" package.

4.3 | Western blot analysis

Total protein extracts were obtained from Arabidopsis lyophilized powder. The powder was resuspended on ice-cold TKMES homogenization buffer (100 mM Tricine-potassium hydroxide pH 7.5, 10 mM KCl, 1 mM MgCl₂, 1 mM EDTA, and 10% [w/v] Sucrose) supplemented with 0.2% (v/v) Triton X-100, 1 mM DTT, 100 µg/ml PMSF, 3 µg/ml E64, and 1X plant protease inhibitor (Sigma). The resuspended sample was centrifuged at 10,000 ×g for 10 min at 4°C and the supernatant recovered for a second step of centrifugation. Protein concentration was determined using the kit Pierce Coomassie Plus (Bradford) Protein-Assay (Thermo Scientific). Approximately 40–50 µg of total protein was separated by SDS-PAGE, transferred to nitrocellulose membrane, and subjected to immunoblotting. The following antibodies were used anti-CCT7 [1:1,000] (Abcam, ab170861) and anti-Actin [1:5000] (Agrisera, AS132640).

4.4 | Separation of soluble and insoluble protein extracts

For the separation of soluble and insoluble (with protein aggregates) fractions, native protein extracts were obtained using a buffer containing 100 mM Tris-HCl pH 7.9, 10 mM MgCl₂, 1% (v/v) glycerol, and 1X plant protease inhibitor (Sigma). After centrifugation for 10 min at 10,000 ×g, the supernatant was collected as the soluble fraction.

The pellet was washed with fresh buffer and centrifuged again. The obtained pellet fraction was then resuspended in denaturing TKMES buffer and centrifuged again to collect the supernatant as the insoluble fraction. Protein concentration from each fraction was determined with Pierce Coomassie Plus (Bradford) Protein-Assay (Thermo Scientific).

4.5 | Filter trap assay

Whole seedlings, root base cells, and root tips containing stem cells were recollected and grinded in liquid N₂. Protein extracts were obtained with native lysis buffer (300 mM NaCl, 100 mM Hepes pH 7.4, 2 mM EDTA, 2% Triton X-100) supplemented with 1X plant protease inhibitor (Sigma). Cellular debris was removed with 80,000 g centrifugation for 10 min at 4°C. Supernatant was recollected and protein concentration determined with Pierce Coomassie Plus (Bradford) Protein-Assay (Thermo Scientific). A cellulose acetate membrane filter (GE Healthcare Life Sciences) was placed in a slot blot apparatus (Bio-Rad) coupled to a vacuum system. Membrane was equilibrated with 3 washes with equilibration buffer (native buffer supplemented with 0.5% SDS). 200 µg of protein extract was supplemented with SDS at a final concentration of 0.5% and loaded and filter through the membrane. Then, the membrane was washed with 0.2% SDS. Retained aggregates of actin were detected using anti-actin antibody [1:5,000] (Agrisera, AS132640). Extracts were also analyzed by SDS-PAGE to determine total actin levels.

4.6 | Blue native gel immunoblotting of TRiC/CCT complex

Whole Arabidopsis seedlings were frozen in liquid nitrogen and ground to powder using a mortar and pestle. The frozen powder was collected in lysis buffer (50 mM Tris-HCl [pH 7.5], 1 mM dithiothreitol and 10% glycerol supplemented with 1X plant protease inhibitor [Sigma]). After centrifugation 10,000 ×g for 10 min at 4°C, the supernatant was collected and protein concentration was determined. 90 µg of total protein was run on a 3–13% gel in deep blue cathode buffer (50 mM Tricine, 7.5 mM Imidazole and 0.02% Coomassie G250) at 4°C for 3 h at 100 V and then exchange deep blue cathode buffer to slightly blue cathode buffer (50 mM Tricine, 7.5 mM Imidazole, and 0.002% Coomassie G250) and run at 100 V overnight. Proteins were then transferred to a polyvinylidene difluoride membrane at 400 mV for 3 h by semi-dry blotting. For loading control, the membrane was stained with Ponceau S. Western blot analysis was performed with a monoclonal antibody against CCT1 [1:1,000] (Abcam, ab109126).

4.7 | Gene expression analysis

Total RNA was extracted from plant tissue, using the Maxwell 16 LEV Plant RNA Kit (Promega). RNA was quantified using a NanoDrop



(Thermo Scientific). cDNA was synthesized using the kit NZY First-Strand cDNA Synthesis Kit (nzytech). SybrGreen real-time quantitative PCR experiments were performed with a 1:20 dilution of cDNA using a CFC384 Real-Time System (Bio-Rad). Data were analyzed with the comparative $2\Delta\Delta C_t$ method using the geometric mean of *Ef1 α* and *PP2A* as housekeeping genes. See Table S1 for qPCR primers used in this work.

4.8 | Confocal microscopy and fluorescence quantification

Confocal microscopy images were taken either with FV1000 Confocal Laser-scanning Microscope (Olympus) or a Meta 710 Confocal Microscope with laser ablation 266 nm (Zeiss). All images were acquired using the same parameters between experiments. For the detection of aggregated proteins, we used the ProteoStat Aggresome detection kit (Enzo Life Sciences). Seedlings were stained according to the manufacturer's instructions. Briefly, seedlings were collected and were fixed in 4% formaldehyde solution for 30 min at room temperature. Formaldehyde solution was removed and seedlings were washed twice with 1X PBS. Then, seedlings were incubated with permeabilizing solution (0.5% Triton X-100, 3 mM EDTA, pH 8.0) with gently shaking for 30 min at 4°C. Seedlings were washed twice with 1X PBS. Then, plants were incubated with 1X PBS supplemented with 1 μ l/ml of ProteoStat and 1 μ l/ml Hoechst 33342 (nuclear staining) for 30 min at room temperature. Finally, seedlings were washed twice with 1X PBS and mounted on a slide. Quantification of ProteoStat fluorescence was performed with ImageJ software.

4.9 | Heat shock survival assay

A single plate containing 6 DAG seedlings (control and CCT8 over-expressor lines) was covered with aluminum foil and transferred to 45°C for 3 h. Then, the plate was transferred back to 22°C under long-day conditions. 108 seedlings were used per line and scored every 3 h. Green seedlings (containing chlorophyll pigments) were considered alive while complete bleached seedlings were considered as dead. PRISM 9 software was used for statistical analysis and *p* values were calculated using the log-rank (Mantel-Cox) method.

ACKNOWLEDGEMENTS

This work was supported by the European Research Council (ERC Starting Grant-677427 StemProteostasis) and the Deutsche Forschungsgemeinschaft (DFG) (Germany's Excellence Strategy-CECAD, EXC 2030-390661388). This work was also supported by a Humboldt Research Fellowship for postdoctoral researchers to E. Llamas. Alga Zuccaro also thanks funding from the Deutsche Forschungsgemeinschaft (SFB-1403-414786233). We thank the technical support from M.R. Rodríguez-Goberna, M. Chmara, and P. Comelli. We thank P. Mammadova and O. Waheed for helping with experiments. We also thank I. Betegón-Putze for helping with

root analysis and measurement. We are grateful to J. Salinas for providing the *pf d 3* and *pf d 5* seeds. Anti-Actin antibody was a gift from J.F. Martínez-García. pGWB502 was a gift from T. Nakagawa (Addgene plasmid 74844). We thank the Salk Institute Genomic Analysis Laboratory and NASC for providing the sequence indexed Arabidopsis T-DNA insertion mutants. We thank the CRAG (M. Amenós) and CECAD (A. Schauss, C. Jungst) imaging facilities for their support in confocal microscopy. Open Access funding enabled and organized by Projekt DEAL.

CONFLICT OF INTEREST

The authors declare no competing interests.

AUTHOR CONTRIBUTIONS

E.L. designed and performed most of the experiments, analyzed the data, and wrote the paper. D.V. planned and supervised the project and wrote the paper. S.T.M., M.V.B., E.S., and N.D. contributed to some of the experiments. H.J.L. performed TRIC/CCT assembly assay. S.T.M. and P.W. analyzed the RNA-seq data. A.Z. and M.R.C. interpreted and discussed the results. W.W., A.Z., and M.R.C. provided reagents and equipment for the research.

DATA AVAILABILITY STATEMENT

There is no restriction on data availability. All data needed to evaluate the conclusions in the paper are present in the paper and/or the Appendix S1.

ORCID

David Vilchez  <https://orcid.org/0000-0002-0801-0743>

REFERENCES

- Ahn, H. K., Yoon, J. T., Choi, I., Kim, S., Lee, H. S., & Pai, H. S. (2019). Functional characterization of chaperonin containing T-complex polypeptide-1 and its conserved and novel substrates in Arabidopsis. *Journal of Experimental Botany*, *70*(10), 2741–2757. <https://doi.org/10.1093/jxb/erz099>
- Balchin, D., Hayer-Hartl, M., & Hartl, F. U. (2016). In vivo aspects of protein folding and quality control. *Science*, *353*(6294), aac4354. <https://doi.org/10.1126/science.aac4354>
- Baurle, I. (2016). Plant heat adaptation: Priming in response to heat stress. *F1000Research*, *5*, 694.
- Betegon-Putze, I., Gonzalez, A., Sevillano, X., Blasco-Escamez, D., & Cano-Delgado, A. I. (2019). MyROOT: A method and software for the semiautomatic measurement of primary root length in Arabidopsis seedlings. *The Plant Journal*, *98*(6), 1145–1156. <https://doi.org/10.1111/tpj.14297>
- Brehme, M., Voisine, C., Rolland, T., Wachi, S., Soper, J. H., Zhu, Y., Orton, K., Villella, A., Garza, D., Vidal, M., Ge, H., & Morimoto, R. I. (2014). A chaperome subnetwork safeguards proteostasis in aging and neurodegenerative disease. *Cell Reports*, *9*(3), 1135–1150. <https://doi.org/10.1016/j.celrep.2014.09.042>
- Clough, S. J., & Bent, A. F. (1998). Floral dip: A simplified method for Agrobacterium-mediated transformation of Arabidopsis thaliana. *The Plant Journal*, *16*(6), 735–743. <https://doi.org/10.1046/j.1365-313x.1998.00343.x>
- Cohen, E., & Taraboulos, A. (2003). Scrapie-like prion protein accumulates in aggresomes of cyclosporin A-treated cells. *EMBO Journal*, *22*(3), 404–417. <https://doi.org/10.1093/emboj/cdg045>



- Dijkwel, P. P., & Lai, A. G. (2019). Hypothesis: Plant stem cells hold the key to extreme longevity. *Translational Medicine of Aging*, 3, 14–16. <https://doi.org/10.1016/j.tma.2018.12.002>
- Douglas, P. M., & Dillin, A. (2010). Protein homeostasis and aging in neurodegeneration. *Journal of Cell Biology*, 190(5), 719–729. <https://doi.org/10.1083/jcb.201005144>
- Durgaprasad, K., Roy, M. V., Venugopal M., A., Kareem, A., Raj, K., Willemsen, V., Mähönen, A. P., Scheres, B., & Prasad, K. (2019). Gradient expression of transcription factor imposes a boundary on organ regeneration potential in plants. *Cell Reports*, 29(2), 453–463 e453. <https://doi.org/10.1016/j.celrep.2019.08.099>
- Finka, A., Mattoo, R. U., & Goloubinoff, P. (2011). Meta-analysis of heat- and chemically upregulated chaperone genes in plant and human cells. *Cell Stress and Chaperones*, 16(1), 15–31. <https://doi.org/10.1007/s12192-010-0216-8>
- Gönczy, P., Echeverri, C., Oegema, K., Coulson, A., Jones, S. J. M., Copley, R. R., Duperon, J., Oegema, J., Brehm, M., Cassin, E., Hannak, E., Kirkham, M., Pichler, S., Flohrs, K., Goessen, A., Leidel, S., Alleaume, A.-M., Martin, C., Özlü, N., ... Hyman, A. A. (2000). Functional genomic analysis of cell division in *C. elegans* using RNAi of genes on chromosome III. *Nature*, 408(6810), 331–336. <https://doi.org/10.1038/35042526>
- Grantham, J. (2020). The molecular chaperone CCT/TRiC: An essential component of proteostasis and a potential modulator of protein aggregation. *Front Genet*, 11, 172. <https://doi.org/10.3389/fgene.2020.00172>
- Green, R. A., Kao, H. L., Audhya, A., Arur, S., Mayers, J. R., Fridolfsson, H. N., & Oegema, K. (2011). A high-resolution *C. elegans* essential gene network based on phenotypic profiling of a complex tissue. *Cell*, 145(3), 470–482. <https://doi.org/10.1016/j.cell.2011.03.037>
- Heyman, J., Kumpf, R. P., & De Veylder, L. (2014). A quiescent path to plant longevity. *Trends in Cell Biology*, 24(8), 443–448. <https://doi.org/10.1016/j.tcb.2014.03.004>
- Hipp, M. S., Kasturi, P., & Hartl, F. U. (2019). The proteostasis network and its decline in ageing. *Nature Reviews Molecular Cell Biology*, 20(7), 421–435. <https://doi.org/10.1038/s41580-019-0101-y>
- Horwich, A. L., Fenton, W. A., Chapman, E., & Farr, G. W. (2007). Two families of chaperonin: Physiology and mechanism. *Annual Review of Cell and Developmental Biology*, 23, 115–145. <https://doi.org/10.1146/annurev.cellbio.23.090506.123555>
- Knowles, T. P., Vendruscolo, M., & Dobson, C. M. (2014). The amyloid state and its association with protein misfolding diseases. *Nature Reviews Molecular Cell Biology*, 15(6), 384–396. <https://doi.org/10.1038/nrm3810>
- Kulkarni, S. R., Vanechoutte, D., Van de Velde, J., & Vandepoele, K. (2018). TF2Network: Predicting transcription factor regulators and gene regulatory networks in Arabidopsis using publicly available binding site information. *Nucleic Acids Research*, 46(6), e31. <https://doi.org/10.1093/nar/gkx1279>
- Lee, H. J., Gutierrez-Garcia, R., & Vilchez, D. (2017). Embryonic stem cells: A novel paradigm to study proteostasis? *FEBS Journal*, 284(3), 391–398. <https://doi.org/10.1111/febs.13810>
- Leeman, D. S., Hebestreit, K., Ruetz, T., Webb, A. E., McKay, A., Pollina, E. A., Dulken, B. W., Zhao, X., Yeo, R. W., Ho, T. T., Mahmoudi, S., Devarajan, K., Passequé, E., Rando, T. A., Frydman, J., & Brunet, A. (2018). Lysosome activation clears aggregates and enhances quiescent neural stem cell activation during aging. *Science*, 359(6381), 1277–1283. <https://doi.org/10.1126/science.aag3048>
- Llamas, E., Alirzayeva, H., Loureiro, R., & Vilchez, D. (2020). The intrinsic proteostasis network of stem cells. *Current Opinion in Cell Biology*, 67, 46–55. <https://doi.org/10.1016/j.ceb.2020.08.005>
- Llamas, E., Pulido, P., & Rodriguez-Concepcion, M. (2017). Interference with plastome gene expression and Clp protease activity in Arabidopsis triggers a chloroplast unfolded protein response to restore protein homeostasis. *PLoS Genetics*, 13(9), e1007022. <https://doi.org/10.1371/journal.pgen.1007022>
- Lopez-Otin, C., Blasco, M. A., Partridge, L., Serrano, M., & Kroemer, G. (2013). The hallmarks of aging. *Cell*, 153(6), 1194–1217. <https://doi.org/10.1016/j.cell.2013.05.039>
- Lundin, V. F., Srayko, M., Hyman, A. A., & Leroux, M. R. (2008). Efficient chaperone-mediated tubulin biogenesis is essential for cell division and cell migration in *C. elegans*. *Developmental Biology*, 313(1), 320–334. <https://doi.org/10.1016/j.ydbio.2007.10.022>
- Martin-Benito, J., Boskovic, J., Gomez-Puertas, P., Carrascosa, J. L., Simons, C. T., Lewis, S. A., & Valpuesta, J. M. (2002). Structure of eukaryotic prefoldin and of its complexes with unfolded actin and the cytosolic chaperonin CCT. *EMBO Journal*, 21(23), 6377–6386. <https://doi.org/10.1093/emboj/cdf640>
- Nakajima, Y., & Suzuki, S. (2013). Environmental stresses induce misfolded protein aggregation in plant cells in a microtubule-dependent manner. *International Journal of Molecular Sciences*, 14(4), 7771–7783. <https://doi.org/10.3390/ijms14047771>
- Noormohammadi, A., Calculli, G., Gutierrez-Garcia, R., Khodakarami, A., Koyuncu, S., & Vilchez, D. (2018). Mechanisms of protein homeostasis (proteostasis) maintain stem cell identity in mammalian pluripotent stem cells. *Cellular and Molecular Life Sciences*, 75(2), 275–290. <https://doi.org/10.1007/s00018-017-2602-1>
- Noormohammadi, A., Khodakarami, A., Gutierrez-Garcia, R., Lee, H. J., Koyuncu, S., König, T., Schindler, C., Saez, I., Fatima, A., Dieterich, C., & Vilchez, D. (2016). Somatic increase of CCT8 mimics proteostasis of human pluripotent stem cells and extends *C. elegans* lifespan. *Nature Communications*, 7, 13649. <https://doi.org/10.1038/ncomms13649>
- Planas-Marques, M., Lema, A. S., & Coll, N. S. (2016). Detection and quantification of protein aggregates in plants. *Methods in Molecular Biology*, 1450, 195–203. https://doi.org/10.1007/978-1-4939-3759-2_15
- Powers, E. T., Morimoto, R. I., Dillin, A., Kelly, J. W., & Balch, W. E. (2009). Biological and chemical approaches to diseases of proteostasis deficiency. *Annual Review of Biochemistry*, 78, 959–991. <https://doi.org/10.1146/annurev.biochem.052308.114844>
- Prahlad, V., & Morimoto, R. I. (2011). Neuronal circuitry regulates the response of *Caenorhabditis elegans* to misfolded proteins. *Proceedings of the National Academy of Sciences*, 108(34), 14204–14209. <https://doi.org/10.1073/pnas.1106557108>
- Prinsloo, E., Setati, M. M., Longshaw, V. M., & Blatch, G. L. (2009). Chaperoning stem cells: A role for heat shock proteins in the modulation of stem cell self-renewal and differentiation? *BioEssays*, 31(4), 370–377. <https://doi.org/10.1002/bies.200800158>
- Pulido, P., Llamas, E., Llorente, B., Ventura, S., Wright, L. P., & Rodriguez-Concepcion, M. (2016). Specific Hsp100 chaperones determine the fate of the first enzyme of the plastidial isoprenoid pathway for either refolding or degradation by the stromal Clp protease in Arabidopsis. *PLoS Genetics*, 12(1), e1005824. <https://doi.org/10.1371/journal.pgen.1005824>
- Pulido, P., Toledo-Ortiz, G., Phillips, M. A., Wright, L. P., & Rodriguez-Concepcion, M. (2013). Arabidopsis J-protein J20 delivers the first enzyme of the plastidial isoprenoid pathway to protein quality control. *The Plant Cell*, 25(10), 4183–4194. <https://doi.org/10.1105/tpc.113.113001>
- Rodriguez-Milla, M. A., & Salinas, J. (2009). Prefoldins 3 and 5 play an essential role in Arabidopsis tolerance to salt stress. *Molecular Plant*, 2(3), 526–534. <https://doi.org/10.1093/mp/ssp016>
- Sablowski, R. (2004). Plant and animal stem cells: Conceptually similar, molecularly distinct? *Trends in Cell Biology*, 14(11), 605–611. <https://doi.org/10.1016/j.tcb.2004.09.011>
- Scheres, B. (2007). Stem-cell niches: Nursery rhymes across kingdoms. *Nature Reviews Molecular Cell Biology*, 8(5), 345–354. <https://doi.org/10.1038/nrm2164>
- Schmid-Siegert, E., Sarkar, N., Iseli, C., Calderon, S., Gouhier-Darimont, C., Chrast, J., Cattaneo, P., Schütz, F., Farinelli, L., Pagni, M., Schneider, M., Voumard, J., Jaboyedoff, M., Fankhauser, C., Hardtke, C. S., Keller, L., Pannell, J. R., Reymond, A., Robinson-Rechavi, M.,



- ... Reymond, P. (2017). Low number of fixed somatic mutations in a long-lived oak tree. *Nature Plants*, 3(12), 926–929. <https://doi.org/10.1038/s41477-017-0066-9>
- Shen, D., Coleman, J., Chan, E., Nicholson, T. P., Dai, L., Sheppard, P. W., & Patton, W. F. (2011). Novel cell- and tissue-based assays for detecting misfolded and aggregated protein accumulation within aggregates and inclusion bodies. *Cell Biochemistry and Biophysics*, 60(3), 173–185. <https://doi.org/10.1007/s12013-010-9138-4>
- Shi, C.-L., von Wangenheim, D., Herrmann, U., Wildhagen, M., Kulik, I., Kopf, A., Ishida, T., Olsson, V., Anker, M. K., Albert, M., Butenko, M. A., Felix, G., Sawa, S., Claassen, M., Friml, J., & Aalen, R. B. (2018). The dynamics of root cap sloughing in Arabidopsis is regulated by peptide signalling. *Nature Plants*, 4(8), 596–604. <https://doi.org/10.1038/s41477-018-0212-z>
- Simmer, F., Moorman, C., van der Linden, A. M., Kuijk, E., van den Berghe, P. V. E., Kamath, R. S., Fraser, A. G., Ahringer, J., & Plasterk, R. H. A. (2003). Genome-wide RNAi of *C. elegans* using the hypersensitive rrf-3 strain reveals novel gene functions. *PLoS Biology*, 1(1), E12. <https://doi.org/10.1371/journal.pbio.0000012>
- Somer, L., Shmulman, O., Dror, T., Hashmueli, S., & Kashi, Y. (2002). The eukaryote chaperonin CCT is a cold shock protein in *Saccharomyces cerevisiae*. *Cell Stress & Chaperones*, 7(1), 47–54.
- Taylor, R. C., Berendzen, K. M., & Dillin, A. (2014). Systemic stress signaling: Understanding the cell non-autonomous control of proteostasis. *Nature Reviews Molecular Cell Biology*, 15(3), 211–217.
- Taylor, R. C., & Dillin, A. (2011). Aging as an event of proteostasis collapse. *Cold Spring Harbor Perspectives in Biology*, 3(5), a004440. <https://doi.org/10.1101/cshperspect.a004440>
- Thiruvalluvan, A., de Mattos, E. P., Brunsting, J. F., Bakels, R., Serlidaki, D., Barazzuol, L., Conforti, P., Fatima, A., Koyuncu, S., Cattaneo, E., Vilchez, D., Bergink, S., Boddeke, E. H. W. G., Copray, S., & Kampinga, H. H. (2020). DNAJB6, a key factor in neuronal sensitivity to amyloidogenesis. *Molecular Cell*, 78(2), 346–358 e349. <https://doi.org/10.1016/j.molcel.2020.02.022>
- Ursic, D., & Culbertson, M. R. (1992). Is Yeast Tcp1 a Chaperonin. *Nature*, 356(6368), 392–392.
- Vallin, J., & Grantham, J. (2019). The role of the molecular chaperone CCT in protein folding and mediation of cytoskeleton-associated processes: Implications for cancer cell biology. *Cell Stress and Chaperones*, 24(1), 17–27. <https://doi.org/10.1007/s12192-018-0949-3>
- van de Hoef, D. L., Bonner, J. M., & Boulianne, G. L. (2013). FKBP14 is an essential gene that regulates Presenilin protein levels and Notch signaling in Drosophila. *Development*, 140(4), 810–819. <https://doi.org/10.1242/dev.081356>
- Vilchez, D., Boyer, L., Lutz, M., Merkwirth, C., Morantte, I., Tse, C., & Dillin, A. (2013). FOXO4 is necessary for neural differentiation of human embryonic stem cells. *Aging Cell*, 12(3), 518–522. <https://doi.org/10.1111/accel.12067>
- Vilchez, D., Boyer, L., Morantte, I., Lutz, M., Merkwirth, C., Joyce, D., & Dillin, A. (2012). Increased proteasome activity in human embryonic stem cells is regulated by PSMD11. *Nature*, 489(7415), 304–308.
- Vilchez, D., Morantte, I., Liu, Z., Douglas, P. M., Merkwirth, C., Rodrigues, A. P. C., Manning, G., & Dillin, A. (2012). RPN-6 determines *C. elegans* longevity under proteotoxic stress conditions. *Nature*, 489(7415), 263–268. <https://doi.org/10.1038/nature11315>
- Vilchez, D., Saez, I., & Dillin, A. (2014). The role of protein clearance mechanisms in organismal ageing and age-related diseases. *Nature Communications*, 5, 5659. <https://doi.org/10.1038/ncomms6659>
- Volovik, Y., Moll, L., Marques, F. C., Maman, M., Bejerano-Sagie, M., & Cohen, E. (2014). Differential regulation of the heat shock factor 1 and DAF-16 by neuronal nhl-1 in the nematode *C. elegans*. *Cell Reports*, 9(6), 2192–2205. <https://doi.org/10.1016/j.celrep.2014.11.028>
- Vonk, W. I. M., Rainbolt, T. K., Dolan, P. T., Webb, A. E., Brunet, A., & Frydman, J. (2020). Differentiation drives widespread rewiring of the neural stem cell chaperone network. *Molecular Cell*, 78(2), 329–345 e329. <https://doi.org/10.1016/j.molcel.2020.03.009>
- Wagle, P., Nikolic, M., & Frommolt, P. (2015). QuickNGS elevates next-generation sequencing data analysis to a new level of automation. *BMC Genomics*, 16, 487. <https://doi.org/10.1186/s12864-015-1695-x>
- Wang, H.-Q., Nakaya, Y., Du, Z., Yamane, T., Shirane, M., Kudo, T., Takeda, M., Takebayashi, K., Noda, Y., Nakayama, K. I., & Nishimura, M. (2005). Interaction of presenilins with FKBP38 promotes apoptosis by reducing mitochondrial Bcl-2. *Human Molecular Genetics*, 14(13), 1889–1902. <https://doi.org/10.1093/hmg/ddi195>
- Weigel, D., & Jurgens, G. (2002). Stem cells that make stems. *Nature*, 415(6873), 751–754. <https://doi.org/10.1038/415751a>
- Wendrich, J. R., Moller, B. K., Li, S., Saiga, S., Sozzani, R., Benfey, P. N., & Weijers, D. (2017). Framework for gradual progression of cell ontogeny in the Arabidopsis root meristem. *Proceedings of the National Academy of Sciences*, 114(42), E8922–E8929. <https://doi.org/10.1073/pnas.1707400114>
- Wong, E., & Cuervo, A. M. (2010). Integration of clearance mechanisms: The proteasome and autophagy. *Cold Spring Harbor Perspectives in Biology*, 2(12), a006734.
- Xu, X. M., Wang, J., Xuan, Z., Goldshmidt, A., Borrill, P. G. M., Hariharan, N., Kim, J. Y., & Jackson, D. (2011). Chaperonins facilitate KNOTTED1 cell-to-cell trafficking and stem cell function. *Science*, 333(6046), 1141–1144. <https://doi.org/10.1126/science.1205727>
- Zheng, P. (2020). Maintaining genomic stability in pluripotent stem cells. *Genome Instability & Disease*, 1(2), 92–97. <https://doi.org/10.1007/s42764-019-00008-4>

SUPPORTING INFORMATION

Additional supporting information may be found online in the Supporting Information section.

How to cite this article: Llamas, E., Torres-Montilla, S., Lee, H. J., Barja, M. V., Schlingens, E., Dunken, N., Wagle, P., Werr, W., Zuccaro, A., Rodríguez-Concepción, M., & Vilchez, D. (2021). The intrinsic chaperone network of Arabidopsis stem cells confers protection against proteotoxic stress. *Aging Cell*, 20, e13446. <https://doi.org/10.1111/accel.13446>

Appendix S1

Supplementary Materials

Figure S1. The cells of the sloughing lateral root cap exhibit high levels of protein aggregates under non-proteotoxic control conditions.

Figure S2. Proteotoxic stress induces protein aggregation in cotyledons.

Figure S3. Proteotoxic stress decreases root growth.

Figure S4. Plants recover growth after removal of proteotoxic stress.

Figure S5. The root apical meristem exhibits high expression of *CCT* subunits.

Figure S6. *CCT* subunits do not increase after heat shock treatment.

Figure S7. Characterization of *cct* mutant lines.

Figure S8. Root length screening assay of Arabidopsis chaperonin mutants.

Figure S9. *cct* mutations result in decreased expression of meristem maintenance markers.

Figure S10. *CCT8* mRNA levels in transgenic 35S:*CCT8* hygromycin-resistant Arabidopsis lines.

Figure S11. Cell-type expression pattern of *CCT8* in the columella and lateral root cap.

Figure S12. Bioinformatics prediction analysis indicate that the transcription factor GATA12 could regulate expression of *CCT* subunits.

Table S1. List of qPCR primers used in this study.

Supplementary Data 1 (separate file)

Analysis of the transcriptome of root cells from the proximal part (mostly stem cells) and distal part (differentiated cells) respect to the QC to identify differentially expressed components of the chaperome network in stem cells.

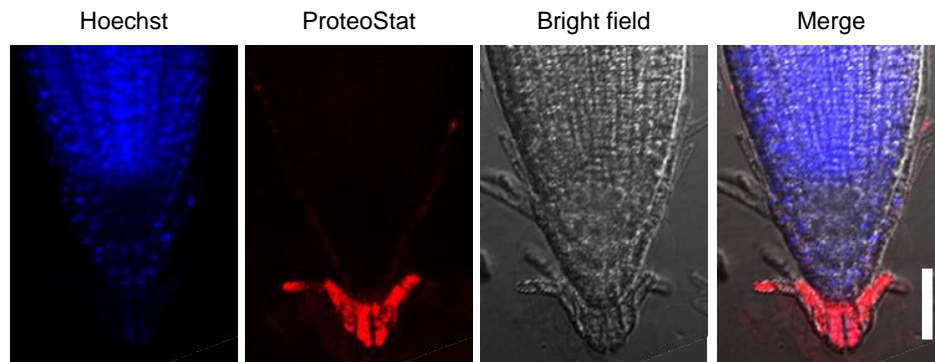


Figure S1. The cells of the sloughing lateral root cap exhibit high levels of protein aggregates under non-proteotoxic control conditions. Representative images of a 6 DAG wild-type root grown at 22°C on plates supplemented with DMSO and stained with ProteoStat. Scale bar indicates 50 μm .

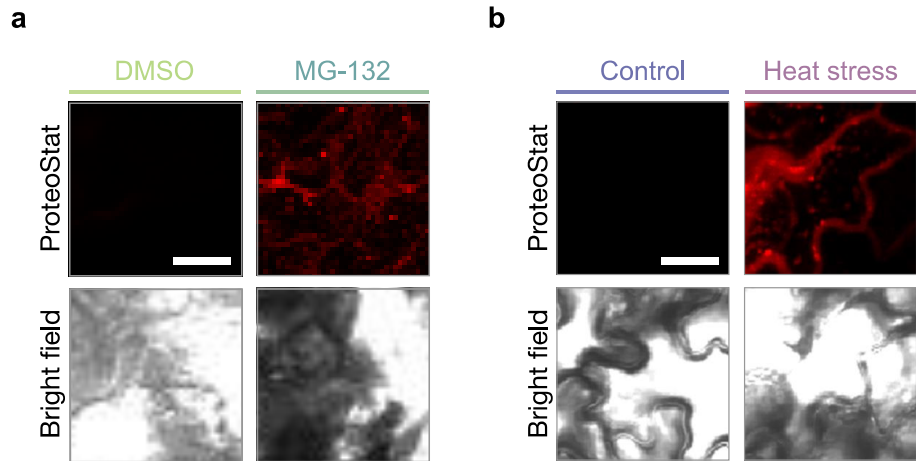


Figure S2. Proteotoxic stress induces protein aggregation in cotyledons. Representative images of cotyledons of plants stained with ProteoStat upon 30 μM MG-132 treatment (a) or heat stress (b). Scale bars represent 20 μm .

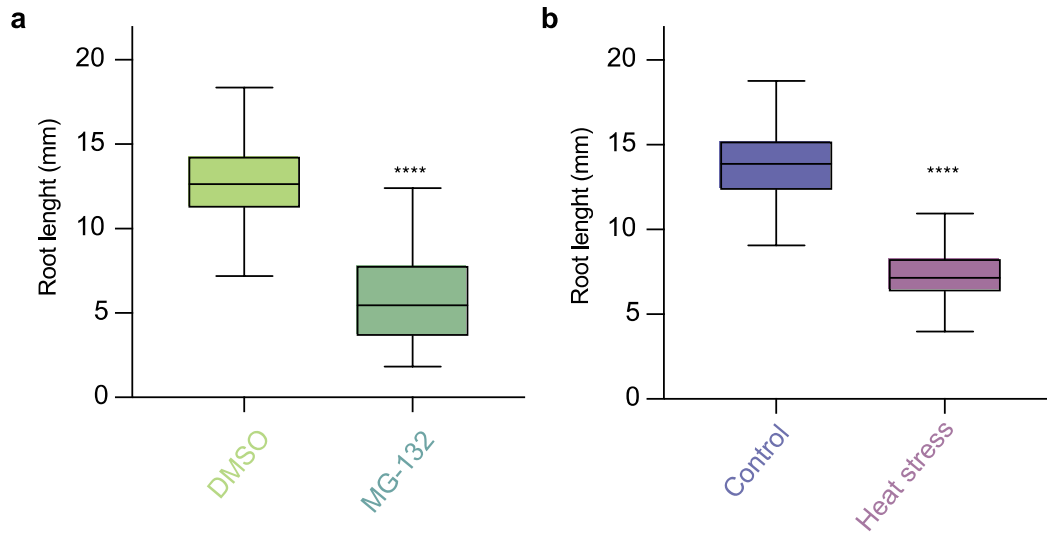


Figure S3. Proteotoxic stress decreases root growth. **a**, Tukey box plots representing root length in millimeters (mm) of 6 DAG Col-0 wild-type plants grown on either DMSO or 30 μ M MG-132 proteasome inhibitor. **b**, Root length of 6 DAG plants grown at 22°C (Control) and 6 DAG plants that were transferred to 37°C at 4 DAG (Heat stress). Horizontal line in Tukey box plots represents the median and box represents 25th and 75th percentiles. Data from 3 independent experiments were analyzed. The statistical comparisons were made by two-tailed Student's *t*-test for unpaired samples. *P* value: **** $P < 0.0001$.

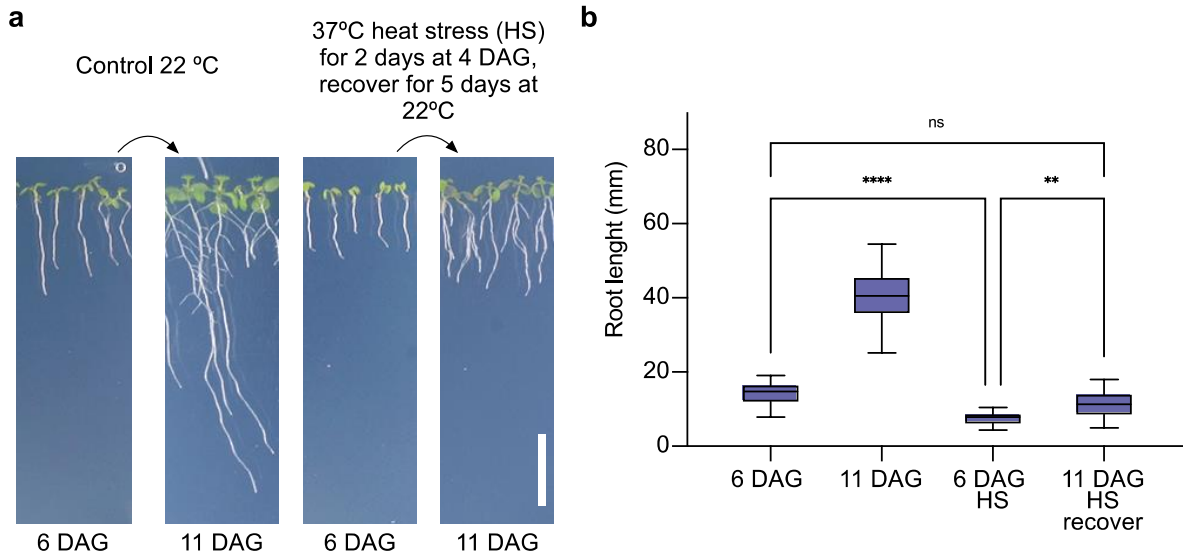


Figure S4. Plants recover growth after removal of proteotoxic stress. **a**, Representative images of 6 DAG or 11 DAG wild-type seedlings grown continuously under control conditions (22°C under long-day conditions) or plants treated with 2 days 37°C heat stress (HS) when they were at 4 DAG stage (grown at 22°C). At 6 DAG heat-treated plants were transfer back to recover at 22 °C for 5 days under long-day conditions. DAG= days after germination. Scale bar represents 10 mm. **b**, Measurement of the root length under the conditions indicated above. Horizontal line in Tukey box plots represents the median and the box represents 25th and 75th percentiles (n= 30). Statistical analysis were performed with one-way ANOVA for multiple comparisons. *P* values: ***P*<0.01, *****P*<0.0001, ns= not significant (*P*>0.05).

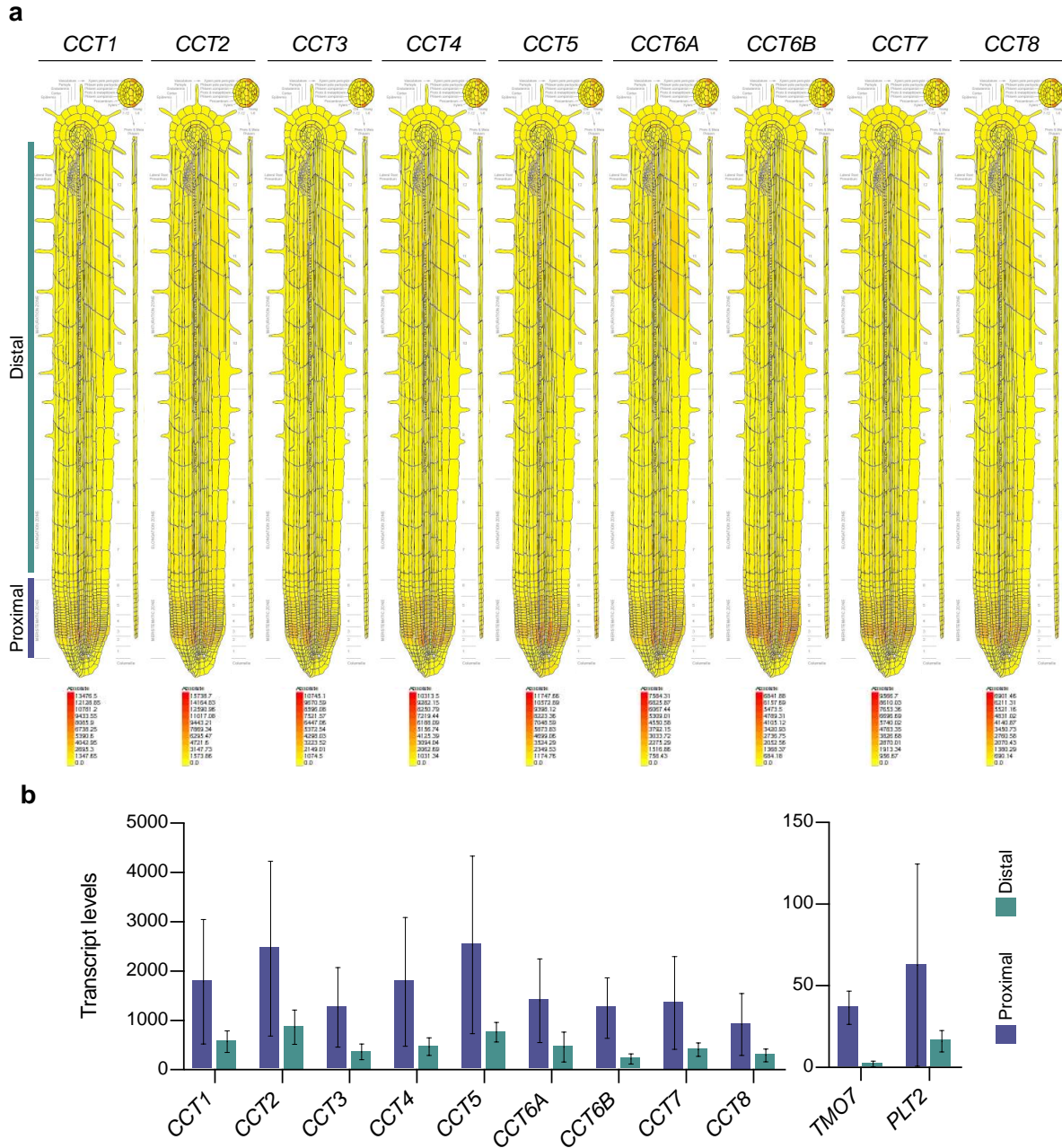


Figure S5. The root apical meristem exhibits high expression of *CCT* subunits. **a**, Root expression maps indicating the spatial level of expression of the distinct Arabidopsis *CCT* subunits. **b**, Bar charts represent the expression levels of *CCT* subunits in xylem corresponding to proximal/young cells (meristematic zone) or distal/old cells (elongation and maturation zone) respective to the QC. The expression levels of the stem cell markers *TMO7* and *PLT2* are also shown. Data obtained from the Arabidopsis Plant eFP Viewer (bar.utoronto.ca). This bioinformatic tool provides gene expression levels and standard deviation, but it does not allow for statistical analysis. In **Figure 2**, we present statistical analysis of RNA-seq and qPCR data supporting that stem cells significantly express higher levels of *CCT*

subunits.

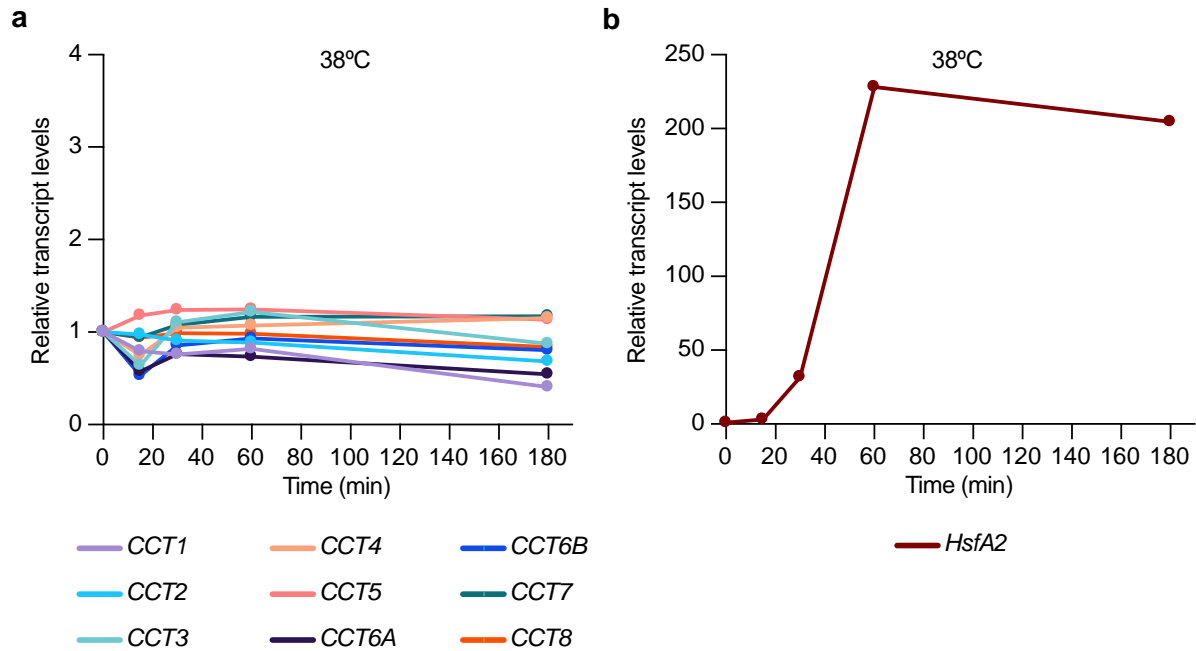


Figure S6. CCT subunits do not increase after heat shock treatment. a, Relative transcript levels of genes encoding CCT subunits after heat shock. Arabidopsis plants grown under long-day conditions were transferred from control condition at 24°C to an incubator at 38°C. Samples from roots were recollected and analyzed at 0, 15, 30, 60, 180 min after transfer to heat stress. **b,** Expression levels of the heat shock regulator *HsfA2* increases rapidly after heat stress exposure. Data obtained from the Arabidopsis Plant eFP Viewer (bar.utoronto.ca).

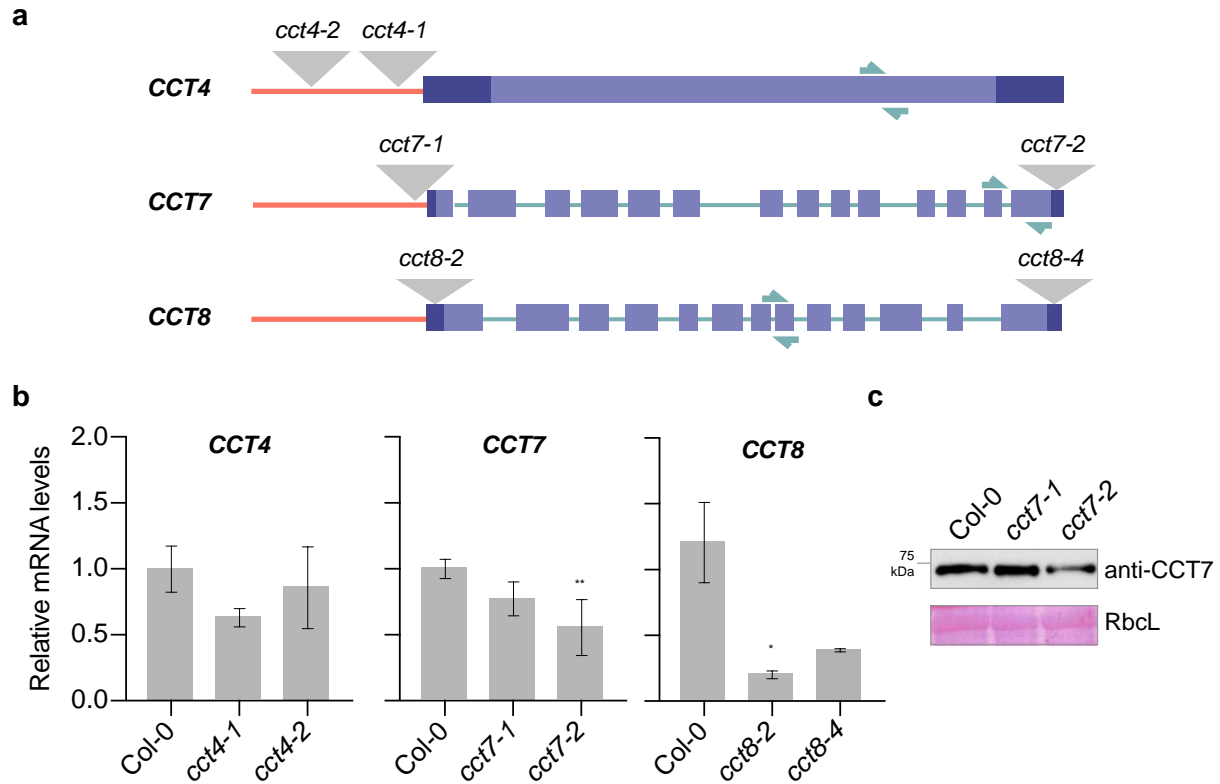


Figure S7. Characterization of *cct* mutant lines. **a**, Schematic representation of the indicated *CCT* genes according to The Arabidopsis Information Resource (TAIR). The promoter region is represented as an orange line, the protein coding sequence (corresponding to the exons) is shown in purple, while the 3' and 5' untranslated regions are shown in dark purple. The approximate T-DNA insertions are represented with gray triangles. Green arrows indicate the position of the qPCR primers used in **Supplementary Fig. 7b**. The schemes are not-to-scale. **b**, qPCR analysis showing transcript levels of the indicated *CCT* genes in 6 DAG *cct* mutants compared to Col-0 wild-type (WT) (mean \pm s.e.m of 3-4 independent experiments). Statistical comparisons were performed by two-tailed Student's *t*-test for unpaired samples. *P* value: **P*<0.05 ***P*<0.01. **c**, Immunoblot with antibody against CCT7 of *cct7* mutants and Col-0 wild-type (15 DAG). Rubisco Large subunit (RbcL) is the loading control. Images are representative of 2 independent experiments.

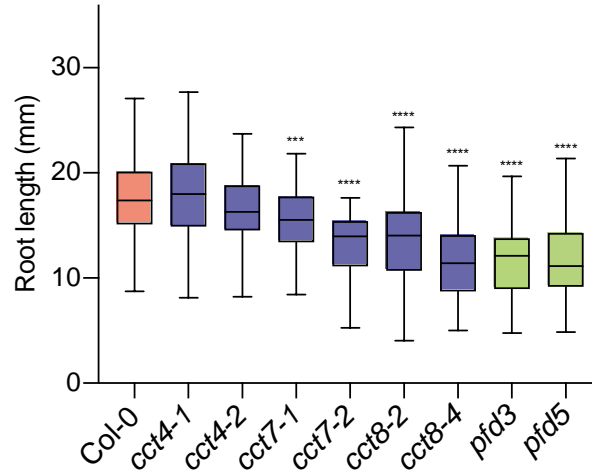


Figure S8. Root length screening assay of Arabidopsis chaperonin mutants. Tukey box plots depicting root length in millimeters (mm) from 6 DAG plants. Horizontal line represents the median, box represents 25th and 75th percentiles. Col-0 (in pink), *cct* (in purple), and *pfd* (in green) mutants were analyzed (n= 25 seedlings from 3 independent experiments). Statistical analysis comparing Col-0 and mutants were performed with one-way ANOVA for multiple comparisons. *P* value: *** $P < 0.001$, **** $P < 0.0001$.

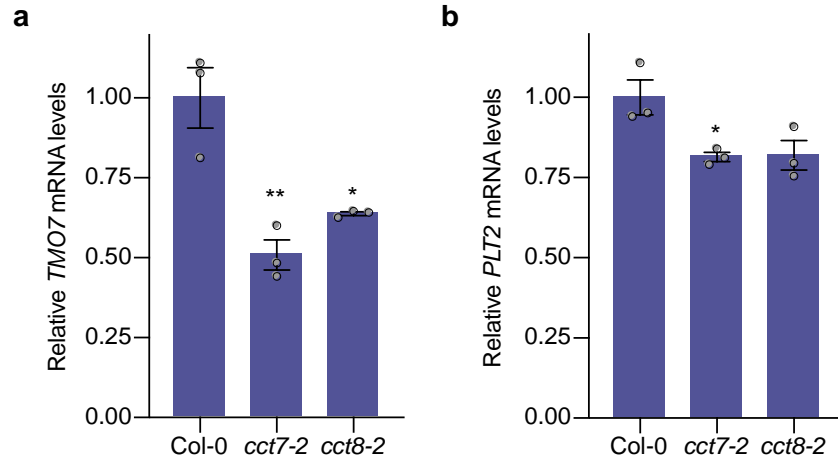


Figure S9. *cct* mutations result in decreased expression of meristem maintenance markers. qPCR analysis showing transcript levels of *TMO7* (a) and *PLT2* (b) genes in 6 DAG seedlings relative to Col-0 (WT). Graphs represent the mean \pm s.e.m of 3 independent experiments. Statistical comparisons were made by two-tailed Student's *t*-test for unpaired samples. *P* value: * $P < 0.05$, ** $P < 0.01$.

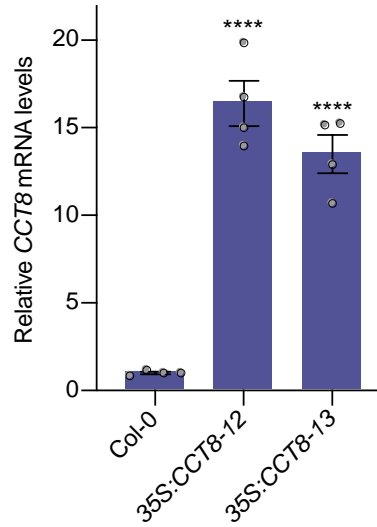


Figure S10. *CCT8* mRNA levels in transgenic *35S:CCT8* hygromycin-resistant *Arabidopsis* lines. qPCR analysis of *CCT8* transcript levels relative to age-matched WT seedlings (6 DAG). Graph represents the mean \pm s.e.m of 4 independent experiments. The statistical comparisons were made by two-tailed Student's *t*-test for unpaired samples. *P* value: **** $P < 0.0001$.

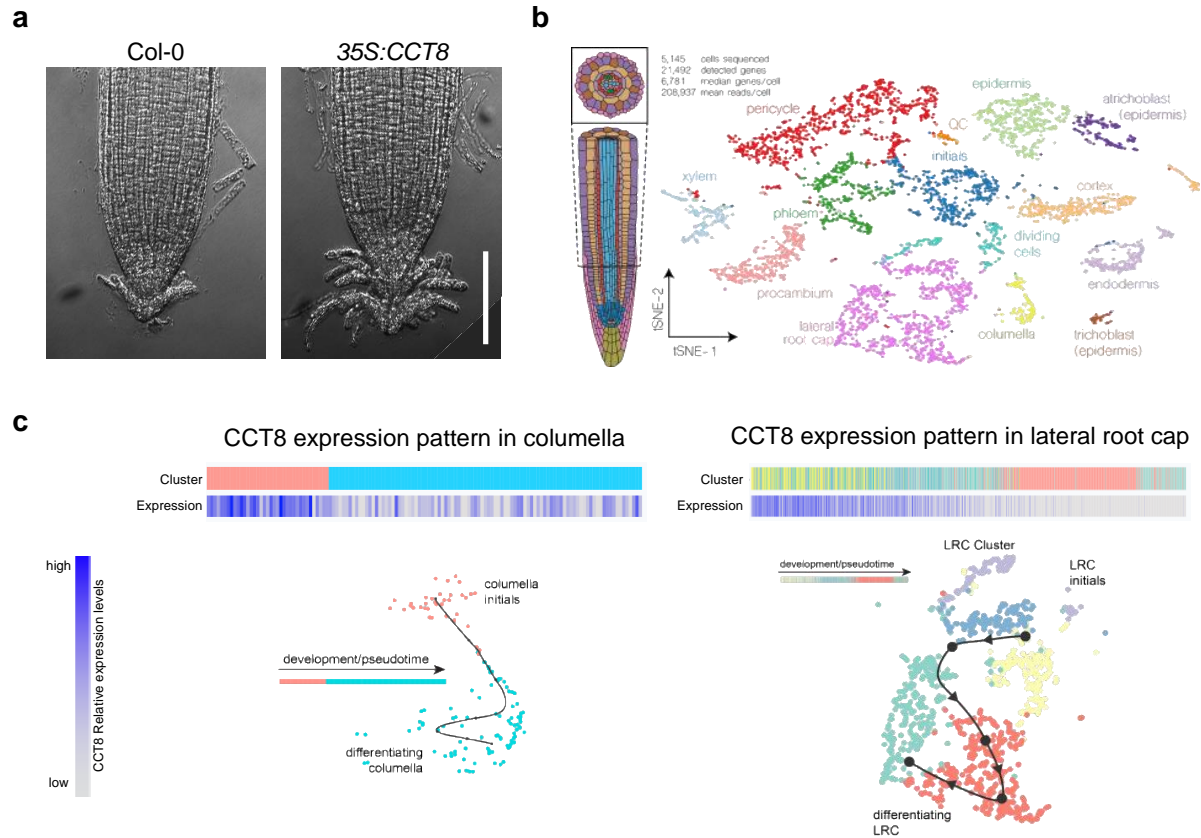


Figure S11. Cell-type expression pattern of *CCT8* in the columella and lateral root cap. **a**, Representative images of the sloughing lateral root cap of Col-0 WT and 35S:*CCT8* grown on plates supplemented with 15 μ M MG-132. **b**, Color-coded tSNE plot showing the classification of 5145 high-quality (UMI count >17,290) cells into distinct cell identities corresponding to the schematic representation of the root meristem on the left. **c**, *CCT8* expression in the columella and lateral root cap decreases during development. Data were obtained from the on-line tool for visualization of cell type specific expression patterns of individual genes along developmental trajectories (<http://bioit3.irc.ugent.be/plant-sc-atlas/>).

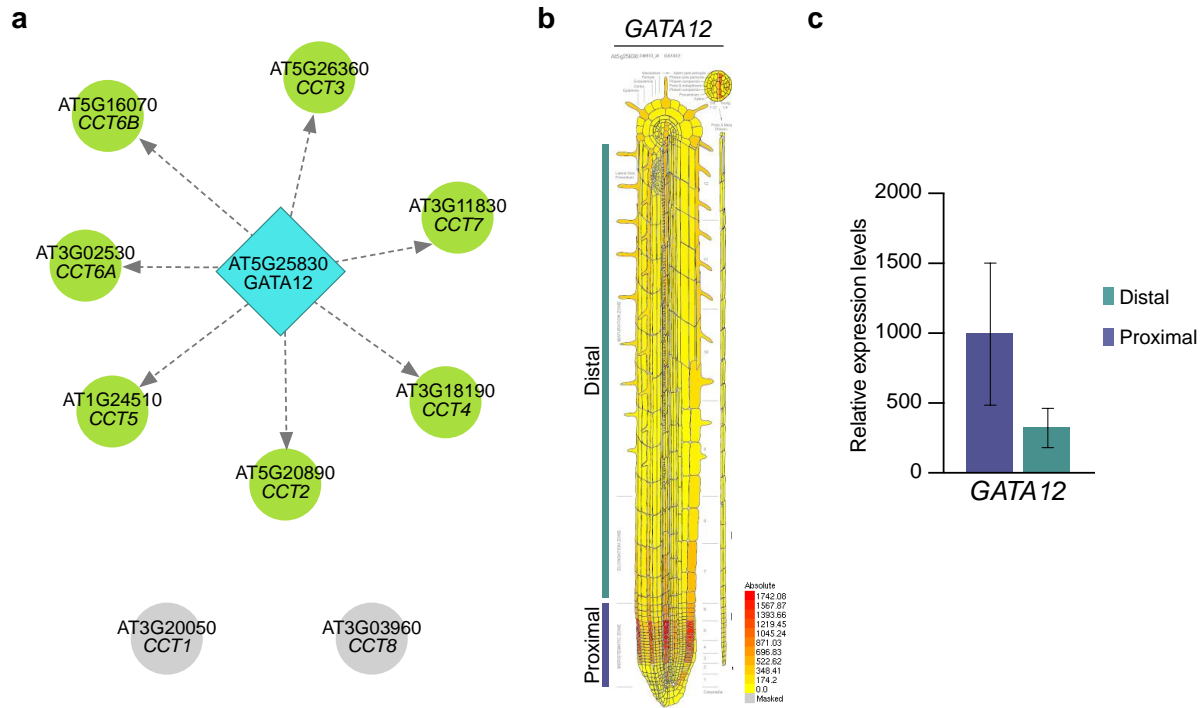


Figure S12. Bioinformatics prediction analysis indicate that the transcription factor *GATA12* could regulate expression of CCT subunits. **a**, *GATA12* is predicted to be a regulator of several CCT genes according to the TF2Network (<http://bioinformatics.psb.ugent.be/webtools/TF2Network/>). In green, *CCT* genes possibly regulated by *GATA12*. In gray, *CCT* subunits that were not predicted to be regulated by *GATA12*. **b**, Root expression map indicating the spatial level of expression of *GATA12*. **c**, Bar chart represent the expression levels \pm standard deviation of *GATA12* in xylem corresponding to proximal/young cells (meristematic zone) or distal/old cells (elongation and maturation zone). Values were obtained from the Arabidopsis Plant eFP Viewer (bar.utoronto.ca).

Gene	AGI Locus	Primers used for qPCR (F/R)	Reference
<i>CCT1</i>	AT3G20050	GTC GGC CTC GAC AAG ATG	Ahn et al., 2019. J Exp Bot. 70: 2741-2757
		CGA CCT CCAACATCC TAA GAA	
<i>CCT2</i>	AT5G20890	CTAAGA TTC ACC CTATGACCA TCA	Ahn et al., 2019. J Exp Bot. 70: 2741-2757
		TTC AGT AAA GCA TTA CGA GCA CA	
<i>CCT3</i>	AT5G26360	CGC TCA TCC TGC AGC TAA GT	Ahn et al., 2019. J Exp Bot. 70: 2741-2757
		ACC AGC TAG AAC AAT AAC AGA CGT T	
<i>CCT4</i>	AT3G18190	AGT GAG CAAAAG GTT TTT GAT TG	Ahn et al., 2019. J Exp Bot. 70: 2741-2757
		ACC GAG CTG CCT TGA GAG	
<i>CCT5</i>	AT1G24510	TTG CTC ACT TGC GGT TGA T	Ahn et al., 2019. J Exp Bot. 70: 2741-2757
		GCA AAC GCC CTA ATT GCA TA	
<i>CCT6A</i>	AT3G02530	AGT GCC TAA GAC GCT TGC TG	Ahn et al., 2019. J Exp Bot. 70: 2741-2757
		TCC TTT GTC ATG CTC ACT CG	
<i>CCT6B</i>	AT5G16070	GAA AGC CTG AGG AAG CTA TTG A	Ahn et al., 2019. J Exp Bot. 70: 2741-2757
		GAA CAA GCC CCT CAA CCA	
<i>CCT7</i>	AT3G11830	CGACTGAAGCGGCTTGCCATCAT	This study
		TATCGCCTTCGCATTCCACGGC	
<i>CCT8</i>	AT3G03960	GTC GCC CAT TTG AAG CTT AG	Ahn et al., 2019. J Exp Bot. 70: 2741-2757
		CTC GTT TCT TGC AAT CGT GA	
<i>TMO7</i>	AT1G74500	CGGGAAGAAGATCACGTTTCGAGGC	This study
		GGAACGACGACTGTCCCTGAGC	
<i>PLT2</i>	AT1G51190	GGTAGGGTATGGAATAATTAGC	Durgaprasad et al., 2019. Cell Rep. 29: 453-463
		CCTAAAAGACTAACCCTCGAG	
<i>EF1α</i>	AT5G60390	CTGGAGGTTTTGAGGCTGGTAT	Wendrich et al., 2017. PNAS. 114: E8922-E8929
		CCAAGGGTGAAAGCAAGAAGA	
<i>PP2A</i>	AT1G13320	TAACGTGGCCAAAATGATGC	Roth et al., 2018. Plant Cell. 30: 1309-1321
		GTTCTCCACAACCGCTTGGT	

Table S1. List of qPCR primers used in this study. Table showing genes, AGI Locus, and primers for qPCR. References where the primers were previously validated for qPCR are also indicated.